(NASA-CR-173269) SUBMILLIMETER ASTRONOMY AT THE NASA/UNIVERSITY OF HAWAII 3-METER INFRARED TELESCOPE FACILITY Final Report, 1 Oct. 1979 - 31 Oct. 1983 (Chicago Univ.) 59 p HC A04/MF A01 CSCL 03A

N84-17083

Unclas G3/89 18254

The University of Chicago

The Enrico Fermi Institute

Final Report

to

The National Aeronautics and Space Administration

on Work under Grant No. NAG-W-4

October 1, 1979 to October 31, 1983

SUBMILLIMETER ASTRONOMY AT THE NASA/UNIVERSITY OF HAWAII 3-METER INFRARED TELESCOPE FACILITY

Roger H. Hildebrand
Principal Investigator

SUBMILLIMETER ASTRONOMY AT THE NASA/UNIVERSITY OF HAWAII 3-METER INFRARED TELESCOPE FACILITY

Final Report. October 1983

I. Introduction

I wish to begin this report by expressing my appreciation to NASA for its support of my submillimeter work at the IRTF during the last few years. I am pleased to offer this report summarizing the fruits of that support. I wish also to say at the beginning that the success of the work has been due in large measure to the efforts of my students Jocelyn Keene and Stanley Whitcomb, now both at Caltech.

In my original proposal of 1979, I said "the NASA/University of Hawaii 3-m Infrared Telescope Facility (IRTF) now nearing completion at MKO is not equipped for work beyond the mid-ir (∿30 μm) but it is feasible to design a submillimeter photometer which would provide for observations at 350 to 1000 μm with higher sensitivities than have been previously obtained at those wavelengths. The excellence of Mauna Kea as a site for submillimeter observations has been demonstrated by our group and others, using the 2.2-m telescope." Accordingly, I proposed "to build a photometer for 350 μm to 1000 μm observations with the 3-meter telescope of the Mauna Kea Observatory and to use the photometer for planetary studies."

Although development of the photometer will continue for some time and a vast opportunity for further application of the photometer to planetary studies still remains, the original goals for this grant have been achieved and a summary is appropriate (regardless of formal requirements for a report).

II. The Photometer

A major problem to be solved in designing a submillimeter photometer for the IRTF was the large focal ratio of the telescope (f/35) and the

corresponding size of the Airy diffraction disk ($2.44\ \lambda f$ = 30 mm at 350 μm; 85 mm at 1000 μm). With apertures of this size, it was essential first of all to provide spectral filters which would thoroughly exclude all wavelengths below the desired passbands and which would not become warm enough to be significant sources of thermal radiation. The filters designed to meet these requirements have been described by Whitcomb and Keene (1980). The arrangement of the filters in the photometer has been described by Whitcomb, Hildebrand, and Keene (1980).

The filtered radiation had still to be concentrated by a very large factor to be coupled to bolometers of reasonable size. We achieved a concentration of $(2f)^2$ = 4,900 using compact heat trap field optics of the type described by Keene, Hildebrand, Whitcomb, and Winston (1978).

The low absorptivity of bolometers for submillimeter radiation and especially near 1 mm has been a continuing problem to which a better solution has recently been found by my graduate student [illegible]k Dragovan (1983). He has shown that a gold film with a surface resistance matching the impedence of free space can produce a superior composite bolometer.

The use of the photometer for a wide variety of applications ranging from studies of solar limb brightening and planetary emission to mapping of dust clouds forced us to make an observational and theoretical analysis of the throughput of diffraction limited field optics systems (Hildebrand and Winston, 1983).

As will be seen from the above discussion, the development of the photometer has stimulated considerable work in applied optics which should be of value to other projects involving detection of submillimeter radiation. I have reviewed the developments in some detail in a recent article (Hildebrand, 1984). The article describing the IRTF photometer (Whitcomb, Hildebrand, and Keene, 1980) is attached to this report as an appendix.

Since the preparation of that article, we have built a ^{3}He-cooled submillimeter photometer as an addition to the IRTF photometer working in collaboration with T. Roellig of Ames Research Center. The next development of the photometer will be the addition of a polarimeter.

The total cost for the design and construction of the photometer (not including the ^{3}He radiometer) is well represented by the sum of the budgets for the first two years (approximately $113,000).

III. Use as a Facility Instrument

Since its first use, the photometer has been used for a series of runs by various groups of observers, usually twice a year. Portions of the instrument, especially the submillimeter radiometer, have been returned to Chicago between each series for improvements. At least one member (or former member) of my group has been present at the beginning of each series to set up and adjust the instrument. I do not have a record of all users. The following is a partial list of those who have observed with the photometer and/or published on investigations using it.

E. Becklin	University of Hawaii
L. Chernig	G.S.F.C.
G. Chin	G.S.F.C.
J. Davidson	University of Chicago (EFI)
M. Dragovan	University of Chicago (EFI)
E. Epstein	Aerospace Corporation
I. Gatley	UKIRT
R. Genzel	University of California, Berkeley
D. Gezari	G.S.F.C.
D. Harper	Yerkes Observatory
R. Hildebrand	University of Chicago (EFI)
D. Jaffe	University of California, Berkeley

M. Jura	U.C.L.A.
J. Keene	Caltech
R. Landau	University of Minnesota
C. Lindsey	University of Hawaii
R. Loewenstein	Yerkes Observatory
G. Novak	University of Chicago (EFI)
G. Orton	J.P.L.
R. Pernic	Yerkes Observatory
L. Rickhard	M.I.T.
T. Roellig	Ames Research Center
P. Schwartz	NRL
K. Sellgren	Caltech
T. Simon	University of Hawaii
H. Smith	NRL
R. Sopka	Catonsville College
C. Telesco	Marshall S.F.C.
M. Werner	Ames Research Center
S. Whitcomb	Caltech
B. Zuckerman	U.C.L.A.

Although we have prepared a fairly detailed operating manual, we expect that the set-up of this instrument will always require the assistance of someone thoroughly familiar with its use. To the extent possible, we will continue to provide such assistance, but we cannot promise to be available or to have the instrument ready at any time.

IV. Planetary Studies

Saturn's Rings

An incentive for rapid completion of the submillimeter component of our photometer was the opportunity to observe Saturn with rings edge-on in

late 1979 and early 1980. By comparing observations at that time with those we had made earlier (at the 2.2-m telescope) when the rings were at an inclination of 20°, we were able to establish a 400 μm brightness temperature for the rings of $T_B(400\ \mu m) = 72 \pm 12$ K, where the error was due primarily to uncertainty in the Mars model used for calibration. (Note that this was before the Saturn fly-by.) This temperature lies between that (90 K) observed for $\lambda \leq 35$ m and that (≤18 K) observed for $\lambda \geq 3.3$ mm. This behavior, combined with the high optical depth of the rings at centimeter wavelengths, placed severe constraints on the size and composition of the ring particles. We concluded that ice particles with sizes of a few centimeters were the most likely candidates.

Titan

At about the time of the Voyager encounter with Saturn we succeeded in measuring the brightness temperature of Titan, thus providing temperature data at an altitude (∿40 km) presumably near the temperature minimum. Our value, 68 ± 6.5 K at 4.5 μm, combined with Voyager and radio occultation data, indicates the presence of a dense, cold cloud layer at that altitude.

Giant Planets

Our most extensive observations were those of the giant planets. Combined with our results from the Kuiper Airborne Observatory taken over the same interval we have obtained brightness temperatures at ten or more passbands in the range 40 μm ≤ λ ≤ 1000 μm for each of the planets Jupiter, Saturn, Uranus, and Neptune. With this broad portion of the spectrum we are able to improve the determination of the total bolometric output of the planets, especially for Uranus and Neptune, where a significant portion of the spectrum is beyond 40 μm.

In addition, since the spectra reflect the temperatures and opacities of the planetary atmospheres down to depths of several bars, we are able to

compare the results with atmospheric models extending to these depths.

A manuscript describing the current status of this work is attached. The data are complete but the manuscript is still being edited by the various authors. This work involves many hundreds of individual observations. The reduction and analysis has proved to be a major task.

V. Other Research

The photometer has been extensively used in solar, galactic, and extragalactic observations. Among the most significant of these were the discovery of low-luminosity star formation in the Bok Globule B335 by Keene et al. (1983) and the determination of the far-infrared properties of dust in the reflection nebula NGC 7023 by Whitcomb et al. (1981).

VI. Publications

The following publications of our group have been based entirely or in part on work under this grant:

An f/35 submillimeter photometer for the NASA Infrared Telescope Facility

S. E. Whitcomb, R. H. Hildebrand, and J. Keene

Pub. A.S.P., 92, 863 (1980)

Far-infrared observations of the globule B335

J. Keene, D. A. Harper, R. H. Hildebrand, and S. E. Whitcomb

Ap. J. (Letters), 240, L43 (1980)

Far-infrared observations of globules

J. Keene

Ap. J., 245, 115 (1981)

Far-infrared properties of dust in the reflection nebula NGC 7023

S. E. Whitcomb, I. Gatley, R. H. Hildebrand, J. Keene, K. Sellgren, and M. W. Werner

Ap. J., 246, 416 (1981)

Brightness temperatures of Saturn's disk and rings at 400 and 700 micrometers

S. E. Whitcomb, R. H. Hildebrand, and J. Keene

Science, 210, 788 (1980)

Solar limb brightening at 350 μm

C. Lindsey, R. Hildebrand, S. Whitcomb, and J. Keene

Ap. J., 248, 830 (1981)

415 μm brightness temperature of Titan

R. F. Loewenstein and R. H. Hildebrand

A. & A., 110, L18 (1982)

The throughput of diffraction-limited field optics systems

R. H. Hildebrand and R. Winston

Applied Optics, 21, 1844 (1982)

A high resolution submillimeter map of OMC-1

J. Keene, R. H. Hildebrand, and S. E. Whitcomb

Ap. J. (Letters), 252, L11 (1982)

The determination of cloud masses and dust characteristics from submillimeter thermal emissions

R. H. Hildebrand

Q. Jl. R. astr. Soc., 24, 267 (1983)

Submillimeter observations of W3

D. T. Jaffe, R. H. Hildebrand, Jocelyn Keene, and S. E. Whitcomb

Ap. J. (Letters), 273, L89 (1983)

Far-infrared detection of low-luminosity star formation in the Bok Globule B335

Jocelyn Keene, J. A. Davidson, D. A. Harper, R. H. Hildebrand, D. T. Jaffe, R. F. Loewenstein, F. Low, and R. Pernic

Ap. J. (Letters), 274, L43 (1983)

Far-IR selected star formation regions

D. T. Jaffe, R. H. Hildebrand, J. Keene, D. A. Harper, R. F. Loewenstein, and J. M. Moran

Ap. J. In press.

Focal plane optics in far-infrared and submillimeter astronomy

R. H. Hildebrand

International Conference on Nonimaging Concentrators, M. C. Ruda, ed. proc. SPIE, 441, 40-50 (1984)

Far-infrared and submillimeter brightness temperatures of the giant planets

R. H. Hildebrand, R. F. Loewenstein, G. Orton, D. A. Harper, J. Keene, and S. Whitcomb

(In preparation)

FAR INFRARED AND SUBMILLIMETER BRIGHTNESS TEMPERATURES OF THE GIANT PLANETS

R. H. HILDEBRAND[1,2,3]

R. F. LOEWENSTEIN[1,2,4]

D. A. HARPER[1,2,4]

G. S. ORTON[5]

J. B. KEENE[1,2,6]

AND

S. E. WHITCOMB[1,2,6]

[1]GUEST OBSERVER: G. P. KUIPER AIRBORNE OBSERVATORY, AMES RESEARCH CENTER, MOFFETT FIELD, CA 94035.

[2]VISITING ASTRONOMER AT THE INFRARED TELESCOPE FACILITY, WHICH IS OPERATED BY THE UNIVERSITY OF HAWAII UNDER CONTRACT FROM THE NATIONAL AERONAUTICS AND SPACE ADMINISTRATION.

[3]ENRICO FERMI INSTITUTE, DEPARTMENT OF ASTRONOMY AND ASTROPHYSICS, AND DEPARTMENT OF PHYSICS, THE UNIVERSITY OF CHICAGO, CHICAGO, IL 60637

[4]DEPARTMENT OF ASTRONOMY AND ASTROPHYSICS, YERKES OBSERVATORY, THE UNIVERSITY OF CHICAGO, WILLIAMS BAY, WI 53191.

[5]JET PROPULSION LABORATORY, CALIFORNIA INSTITUTE OF TECHNOLOGY, 4800 OAK GROVE DRIVE, PASADENA, CA 91109.

[6]DIVISION OF PHYSICS, MATHEMATICS, AND ASTRONOMY, CALIFORNIA INSTITUTE OF TECHNOLOGY, PASADENA, CA 91125.

ORIGINAL PAGE IS
OF POOR QUALITY

ABSTRACT

WE HAVE MEASURED THE BRIGHTNESS TEMPERATURES OF JUPITER, SATURN, URANUS, AND NEPTUNE IN THE RANGE 35-1000 μM. THE EFFECTIVE TEMPERATURES DERIVED FROM THE MEASUREMENTS, SUPPLEMENTED BY SHORTER WAVELENGTH VOYAGER DATA FOR JUPITER AND SATURN, ARE 126.8 ± 4.5 K, 93.4 ± 3.3 K, 58.3 ± 2.0 K, AND 60.3 ± 2.0 K RESPECTIVELY. WE DISCUSS THE IMPLICATIONS OF THE MEASUREMENTS FOR BOLOMETRIC OUTPUT AND FOR ATMOSPHERIC STRUCTURE AND COMPOSITION. THE TEMPERATURE SPECTRUM OF JUPITER SHOWS A STRONG PEAK AT ~ 350 μM FOLLOWED BY A DEEP VALLEY AT ~ 450 - 500 μM. A MODEL ATMOSPHERE CONTAINING AMMONIA ICE PARTICLES REPRODUCES THESE QUALITATIVE FEATURES BUT DOES NOT FIT THE DATA CLOSELY.

I. INTRODUCTION

Far-infrared and submillimeter photometric observations of the giant planets have three principal types of applications: first, the investigation of internal sources of energy; second, the investigation of planetary atmospheres; and third, the establishment of convenient reference objects for photometry of other sources.

The application of planet data to general infrared photometry becomes increasingly valuable as measurements are extended throughout the far-IR and submillimeter spectrum with enough resolution to show the principal features of the spectrum. As we will show, the assumption of a featureless spectrum could lead in some cases to considerable errors.

The atmospheres of the planets are probed to increasing depths by observations at increasing wavelengths. Atmospheric models can be compared with brightness temperature spectra by summing the contributions from each layer of the model atmosphere where each contributes according to its temperature and opacity and the attenuation of its emission by overlying layers. We shall discuss the implications of our measured spectra for the derivation of models for each of the planets at layers down to approximately the one-bar level.

Our measurements permit a considerable reduction in the uncertainties associated with the bolometric thermal outputs of the planets. For Uranus and Neptune, the bulk of the thermal emission occurs in the range 40 μm to 1 mm 35
covered by our observations.

Spacecraft observations have provided measurements of Jupiter and Saturn out to approximately 50 μm (Hanel et al. 1979, Hanel et al. 1982). Airborne observations have extended the spectra to ~100 μm (Loewenstein et al. 1977a, Loewenstein et al. 1977b) and ground-based observations have given a few

broadband points at longer wavelengths short of 1 mm (Loewenstein et al. 1977a, Whitcomb et al. 1979). The measurements presented here cover the range from 35 to 1000 μm in relatively narrow bands. The airborne (35–330 μm) and ground-based (350–970 μm) observations were made at approximately the same times. In these measurements, we have sampled roughly 50% of the total flux emitted by Jupiter, 65% by Saturn, and 92% by Uranus and Neptune.

In the following sections we present the observations and instrumentation II); the data reduction, including corrections, calibration, and planetary radii (III); the results (IV); discussion of models of the individual planets (V); and a summary (VI). Certain details of the analysis are presented in appendices.

II. OBSERVATIONS AND INSTRUMENTATION

The observations were made in ten or more wavelength bands between 35 μm and 970 μm for each planet. The observations at $\lambda \geq 350$ μm were made at the 3 m NASA Infrared Telescope Facility (IRTF) of the Mauna Kea Observatory; those at $\lambda < 350$ μm were made with the Kuiper Airborne Observatory (KAO) The observations extended over the period 1979 November to 1982 September. All the observations of Saturn were made between 1979 November 27, 1980 May 7 when the ring inclination to earth was $< 1^\circ.7$.

(a) IRTF

The IRTF data were obtained in approximately 330 individual observations during the period 1979 November to 1981 March. Flux densities were obtained in six wavelength bands from 350 to 1000 μm using the University of Chicago Submillimeter/Millimeter Photometer (Whitcomb, Hildebrand and Keene 1980). The signals were obtained by repetitive beam switching with a beam separation of 300 arc sec.

Figure 1 shows the transmission curves of the filters as measured on a Fourier transform spectrometer. The apertures were 60 mm for the 1 mm filter (M2) and 29 mm for all submillimeter filters. (Plate scale ~ 2"/mm).

The measurements with the various submillimeter filters were made in a regular sequence designed to reduce errors due to changes in air mass. The sequence is described in Appendix C.

(b) KAO

The airborne observations were made on the 91-cm telescope of the KAO during the period 1980 January, to 1982 September. Three helium cooled photometers were used: photometers G1 and S1 each contained a single detector and photometer G2 consisted of a close packed hexagonal array of seven detectors (one central detector surrounded by six) (Harper et al. 1984). The

FILTERS AND APERTURES IN PHOTOMETERS G1 AND G2 (HARPER ET AL., 1984) INCLUDED BOTH BANDPASS AND LONG-WAVELENGTH PASS FILTERS. FILTERS G1-5, G1-6, G2-5 AND G2-6 HAVE SHORT WAVELENGTH LEAKS OF A FEW PERCENT OR LESS BETWEEN 20 μM - 50 μM. THESE LEAKS REQUIRE CORRECTIONS UP TO 15% IN FLUX RATIOS WHEN COMPARING OBJECTS OF SIGNIFICANTLY DIFFERENT TEMPERATURES. FOR MANY OF THE OBSERVATIONS, WE WERE ABLE TO SWITCH IN ADDITIONAL TEFLON OR CALCIUM FLOURIDE FILTERS WHICH RENDERED THE LEAKS COMPLETELY NEGLIGIBLE. (SEE FOOTNOTES (F) AND (G) OF TABLE IV FOR SPECIFIC NOTES ON FILTERS.)

THE TWO WATER RADIOMETERS ON BOARD THE KAO ARE DESCRIBED BY KUHN ET AL. (1976). FOR SPECIFIC NOTES ON THE WATER VAPOR MEASUREMENTS DURING THE AIRBORNE OBSERVATIONS, REFER TO FOOTNOTE (A) OF TABLE IV. THE DEPENDENCE OF THE ATMOSPHERIC TRANSMISSION FUNCTION UPON THE LINE OF SIGHT WATER VAPOR WAS CALCULATED BY STIER (1983 - PRIVATE COMMUNICATION) BASED UPON THE MODEL OF TRAUB AND STIER (1976).

III. DATA REDUCTION

(A) CORRECTIONS, ANALYSIS

THE SIGNALS HAVE BEEN CORRECTED FOR PARTIAL RESOLUTION OF THE PLANETARY DISKS (APPENDIX A), FOR SHADOWING OF SATURN'S DISK BY THE RINGS (APPENDIX B), AND FOR ATMOSPHERIC TRANSMISSION AND THE SPECTRAL RESPONSE OF THE PHOTOMETERS (APPENDIXES C, D). THE CORRECTION FOR PARTIAL RESOLUTION DOES NOT INCLUDE THE EFFECT OF LIMB DARKENING; THE EFFECT OF THIS SIMPLIFICATION IS ESTIMATED IN APPENDIX A. BECAUSE THE RING INCLINATION WAS LESS THAN 1.7° FOR ALL OBSERVATIONS, NO CORRECTION IS MADE FOR EMISSION FROM SATURN'S RINGS.

FOR THE IRTF DATA, ALL SIGNALS ARE CORRECTED TO THE SAME VALUES OF THE LINE OF SIGHT WATER VAPOR, W, BEFORE TAKING RATIOS OF UNKNOWN TO CALIBRATION

signals (w = 1 mm H_2O for submillimeter measurements, 5 mm H_2O for millimeter measurements; see Appendix D). For the KAO data, the atmospheric corrections of individual measurements were much lower. The spectra of the unknown and calibration sources were assumed to be similar in gross features for $\lambda \gtrsim 350$ µm, but the source spectra of cold and warm planets (e.g. Neptune and Mars) were not similar even in their gross features for $\lambda << 100$ µm. It was therefore necessary to use different analysis procedures for the IRTF and KAO data. See Appendix D for description of the IRTF data reduction and Loewenstein et al. (1977a) for the KAO procedure.

(b) Effective Wavelength

The detection efficiency at frequency ν with line of sight water vapor w depends on the atmospheric transmission, $T(\nu, w)$ and on the measured spectral response of the photometer $A(\nu)$. For a source of spectrum $S(\nu)$, we define a flux weighted mean frequency for the i^{th} filter to be

The wavelengths shown in the tables and figures are those corresponding to the mean frequencies so defined (i.e. $\lambda_I = c/\langle\nu\rangle_I$).

(c) Brightness Ratios

Brightness ratios are calculated from the signal ratios using the planet radii discussed in Section IIIe after corrections for partial resolution of the disk and the inclination of the planet pole.

(d) Calibration: Mars Model

Temperatures are derived from the brightness ratios using Mars as the primary calibration object. The Mars temperatures are based on the model of Neugebauer et al. (1971) as extended by Wright (1976) and further extended and tabulated by Wright and Odenwald (1980). The model g. a decreasing dependence of temperature on wavelength as the wavelength increases. We have

ORIGINAL PAGE IS OF POOR QUALITY

assumed $T(\lambda > 350\ \mu m) = T(\lambda = 350\ \mu m)$. The errors shown in the tables do not include any estimate of the uncertainty in the model.

We do not attempt to evaluate the accuracy of the Wright/Odenwald model. We have, however, compared that model with the more detailed model of Simpson et al. (1981). For the times of the observations, the Mars temperatures of the two models were very nearly equal for $\lambda < 80\ \mu m$. The discrepencies are smaller than the errors we estimate for the measurements. At increasing wavelengths the temperatures of the Simpson model decrease less rapidly than those of the Wright/Odenwald with a discrepency of ~ 7 K at 300 μm. We have assumed the Wright/Odenwald model because it is more easily generated for a given epoch and because it has been widely used as a standard. Major discrepencies in the model would be apparent by their effect on the internal consistency of the planet data.

(e) Planetary Radii

Published direct observations of planetary radii have been made at different wavelengths for the different planets and hence correspond to different depths in the atmospheres. The discrepencies are of order one percent in radius. For consistency, we use radii computed for 1 bar pressure levels which should be approximately the mean radii for the far IR and SMM emission.

For Jupiter, we use the 100-mbar values $R_{EQ} = 71541 \pm 4$ km and $R_{POL} = 66896 \pm 4$ km of Lindal et al. (1981). These values were adjusted to the 1-bar level ($Z = 46$ km) with a mean of the Lindal et al. models (e.g. the nominal model given by Orton, 1981). For Saturn, we use the 182.2-mbar radius, $R_{EQ} = 60309.5$ km, and ellipticity, $\varepsilon = 0.096$, of Kliore et al. (1980) adjusted to the 1-bar level ($Z = 76.6$ km) with a model approximating the preliminary results

of Tyler et al. (1982). For Uranus, we use the 8×10^{13} cm^{-3} (approximately 1 bar) values $R_{EQ} = 26156 \pm 30$ km and $\varepsilon = 0.024 \pm 0.003$ given by Elliott et al. (1981) The adjustment to the 1-bar level ($Z = 582$ km) is based on the models of Tokunaga et al. (1983). For Neptune, we use the 4×10^{13} cm^{-3} values $R_{EQ} = 25225 \pm 30$ km and $\varepsilon = 0.021 \pm 0.004$ given by Elliot (1979), adjusted to the 1-bar level ($Z = 465$ km), again on the basis of the atmospheric models of Tokunaga et al. (1982). These atmospheric models for Uranus and Neptune, while constrained by recent infrared data in the 20 μm region, imply altitude adjustments close to those derived from the equilibrium models of Appleby (1980) or Wallace (1980). The largest uncertainty in the radius adjustments for Uranus and Neptune stems from the uncertainty in the mean molecular weight. We assume a bulk composition of 90% H_2 and 10% He, consistent with the stellar occultation analyses. There are no firm observational constraints on the bulk compositions of Uranus or Neptune. A 10% change in the He mixing ratio translates into a change in the radius adjustment of approximately 50 km.

With these adjustments, we obtain the assumed 1-bar radii listed in Table I.

For Mars, we use the triaxial ellipsoid fit of Sweetnam, (1980) with a polar radius 3377.1 km and equatorial components 3393.5 km and 3400.0 km. We use $R_{EQ} = (3393.5 \times 3400.0)^{1/2} = 3397$ km.

The effective semi-diameters of the planets, Φ , shown in Tables II - IV, are computed from the radii in Table I taking into account the inclinations of the planet poles to the line of sight on the dates of the observations. The range of angles during the observations is shown for each planet in the last column of Table I. The pole coordinates are based on the report of Davies et al. (1980) as presented in the 1982 Astronomical Almanac.

ORIGINAL PAGE IS
OF POOR QUALITY

IV. RESULTS

THE JOURNALS OF THE OBSERVATIONS ARE GIVEN IN THREE SEPARATE PARTS: BROADBAND IRIS OBSERVATIONS (TABLE II), NARROWER BAND IRTF OBSERVATIONS (TABLE III), AND KAO OBSERVATIONS (TABLE IV). THE BRIGHTNESS TEMPERATURE MEASUREMENTS ARE COMBINED AND SUMMARIZED IN TABLE V. THE COMBINED RESULTS ARE PLOTTED IN FIGURES 2 - 5 TOGETHER WITH CURVES REPRESENTING ADJUSTMENTS OF SEMI-EMPIRICAL MODELS FITTED TO THE DATA. THE ORIGINAL MODELS FOR JUPITER AND SATURN ARE BASED ON THOSE OF THE VOYAGER IRTF TEAM (E.G. HANEL ET AL. 1981, 1983) DERIVED FROM DATA TAKEN FOR λ <50 μM; THE MODELS FOR URANUS AND NEPTUNE ARE THOSE OF TOKUNAGA ET AL. (1983). THE DATA WERE FIRST REDUCED USING THESE MODELS (DASHED CURVES). THE DEVIATIONS OF THE REDUCED DATA POINTS FROM THE ASSUMED CURVE WERE FITTED BY A SMOOTH FUNCTION THAT WAS THEN USED TO ADJUST THE ORIGINAL MODEL TO MINIMIZE THE DEVIATIONS. WHEN NECESSARY, THIS NEW SOURCE CURVE WAS THEN USED TO RE-REDUCE THE ORIGINAL RATIOS FOLLOWING THE PROCEDURE DESCRIBED IN THE APPENDIX OF JAFFE ET AL (1984). THIS PROCEDURE REQUIRED TWO ITERATIONS FOR JUPITER, ONE FOR SATURN AND URANUS, AND NONE FOR NEPTUNE. THE NON-UNIQUE FINAL CURVES ARE SHOWN IN THE FIGURES (SOLID CURVES), WITH THE PLOTTED POINTS BEING DERIVED FROM THESE CURVES. IT SHOULD BE STRESSED THAT THESE CURVES DO NOT NECESSARILY REPRESENT A REAL DESCRIPTION OF THE PLANET'S THERMAL STRUCTURE, BUT RATHER REPRESENT THE BEST FIT TO OUR DATA, WHICH RELY ON AN ASSUMED MARS MODEL AND OBSERVATIONAL ERRORS.

THE NUMBER OF INTEGRATIONS USED IN MEASURING THE AIRBORNE POINTS WAS USUALLY TOO SMALL TO PERMIT ESTIMATES OF STATISTICAL ERRORS FOR INDIVIDUAL POINTS. WHERE ERRORS COULD BE ESTIMATED, THEY ARE SHOWN IN TABLE IV. SINCE ALL AIRBORNE MEASUREMENTS ARE SHOWN IN FIGURES 2-5, THE SPREAD CAN BE USED TO JUDGE TYPICAL ERRORS. THE PRINCIPAL SOURCES OF SYSTEMATIC ERRORS FOR THESE POINTS ARE UNCERTAINTIES IN ATMOSPHERIC WATER VAPOR (AIRBORNE DATA) AND

uncertainty in the Mars model (all data). We emphasize that none of the errors shown in the tables include the uncertainty in the Mars reference temperatures. We assume an absolute accuracy to ± 15% in flux. The averages and statistical errors of the combined data points are tabulated in Table V. The average of the airborne statistical errors is 1.5 K and represents the average statistical error in any given airborne measurement.

Since the actual measurements are those of flux, we plot the individual airborne points and the combined groundbased points in Fig. 6 for each planet, normalized to a fixed planetary solid angle. This representation offers a better feel for the various observational errors.

Recent unpublished measurements by Holt et al. (1984) in the range 350 µm to 3.3 mm are generally in fair agreement with our data, but somewhat lower. Only a small part of the difference can be explained by differences in assumed Mars reference temperatures. The principal discrepancy is in the Jupiter data in the region 350 µm-500 µm, where our points are higher and show a strong peak at ~350 µm followed by a valley at ~450 µm. We do not understand the reason for the discrepancy.

Integrating the curves in Figure 6 and correcting for unmeasured flux short of 35 µm, one arrives at T_{EFF} for Jupiter, Saturn, Uranus and Neptune to be respectively 126.8 ± 4.5 K, 93.4 ± 3.3 K, 58.3 ± 2.0 K, and 60.3 ± 2.0 K. Here the errors represent the assumed 15% error in flux due to the uncertinties in the Mars temperatures.

V. DISCUSSION

Various models can be constructed for the spectra of the Giant Planets. Details of the compositional and structural assumptions characterizing each model, as well as descriptions of the analysis, are discussed at greater length

IN APPENDIX E. RESULTS OF THESE MODELS ARE DESCRIBED BELOW.

A. JUPITER

EARTH-BASED OBSERVATIONS OF JUPITER HAVE BEEN MADE BY PHOTOMETRIC AND SPECTROSCOPIC TECHNIQUES. MOST RECENTLY THE VOYAGER IRIS EXPERIMENT OBTAINED MANY SPECTRA OF JUPITER (HANEL ET AL. 1979), INCLUDING SOME OBSERVATIONS OF THE WHOLE DISK (HANEL ET AL. 1981) OUT TO 50 μM. THESE SPECTRA ARE ESSENTIALLY COINCIDENTAL WITH THE MODEL SPECTRA DISPLAYED IN FIGS. 7-9.

FIG. 7 INCLUDES THE SPECTRUM OF A MODEL ATMOSPHERE WITHOUT ACCOUNTING FOR THE INFLUENCE OF NH_3 ICE CLOUDS, AS WELL AS ONE WITH NH_3 CLOUDS HAVING A CHARACTERISTIC PARTICLE SCALE HEIGHT EQUAL TO 0.15 TIMES THE GAS SCALE HEIGHT. FIGS. 8 AND 9 SHOW THE SPECTRA RESULTING FROM SIMILAR CLOUDS WITH PARTICLE SCALE HEIGHTS EQUAL TO 0.50 AND 0.05 TIMES THE GAS SCALE HEIGHT, RESPECTIVELY. THE MODELS ARE EXTENSIONS OF THOSE PRESENTED BY ORTON ET AL. (1982B). NONE OF THESE MODELS GIVES A CLOSE FIT TO THE DATA NEAR THE 350 - 700 MICRON REGION FOR ANY PARTICLE SIZE CONSIDERED, EVEN WHEN A DETAILED RESPONSE TO THE PREDICTED SPECTRUM IS CONSIDERED.

IF THE DATA ARE CORRECT, OTHER SOURCES OF JOVIAN ATMOSPHERIC ABSORPTION MAY BE REQUIRED. FUTURE OBSERVATIONAL EFFORTS MAY BEST BE DIRECTED TOWARD OBTAINING SPECTROMETRIC RATHER THAN RADIOMETRIC DATA. THIS WOULD ELIMINATE THE UNCERTAINTY IMPLICIT IN THE CONVOLUTION OF STRONG TELLURIC AND JOVIAN ABSORPTION FEATURES.

ALTHOUGH THEY ARE ONLY WEAKLY CONSTRAINED BY THE DATA, THE CLOUDY MODELS IN FIGS. 7-9 MAY BE USED TO OBSERVE BY VOYAGER FOR WAVELENGTHS BEYOND 43.5 μM ($0 - 230\ cm^{-1}$). OUR CLOUDY MODELS PREDICT VALUES OF $1.51 - 1.54 \times 10^{4}\ W\ cm^{-2}$ $ster.^{-1}$ FOR THE $0 - 230\ cm^{-1}$ FLUX. THESE INDICATE AN AVERAGE WHICH IS ONLY 2% HIGHER THAN THE ESTIMATE OF $1.507 \times 10^{-4}\ W\ cm^{-2}\ ster.^{-1}$ GIVEN BY HANEL ET AL.

(1981). The average of our models tends to confirm the estimate of the total thermal output of 4 325 × 10^4 W cm^{-2} ster.$^{-1}$ given by Hanel et al. They also confirm the 2% estimate for their long wavelength extrapolation uncertainty.

B. Saturn

Fig. 10 shows the spectra of models for Saturn with a PH_3 mixing ratio in the deep atmosphere of 1.5 × 10^{-6}, corresponding to the results of earlier investigations (see Appendix E). Models with larger mixing ratios are also shown to demonstrate the influence of PH_3 lines in this region of the spectrum. The measurements at 204.3, 221.1 and 328.9 μm all appear to be below the model spectra and could be interpreted as indicating that larger mixing ratios are required or that there is an unmodeled absorber influencing the spectrum. On the other hand, other measurements, such as the datum at 664 μm which lies above the model spectrum, are not so easily explained. Again, just as for Jupiter, this spectral region is sufficiently detailed that unambiguous extraction of information about the atmosphere of Saturn may require spectrometric rather than radiometric observations.

We note that the model spectra in Fig. 13 do provide a reasonably satisfactory fit to the data, and they do not indicate the need for a decrease in the model brightness across a wide spectral range. The cloud models suggested by Orton (1983) for regions near the equator and near 15°S latitude are thus optically too thick for the global average. This may be a result of the contribution of the relatively bright and "clear" regions in the northern hemisphere (Pirraglia et al. 1981; Gautier et al. 1983).

Finally, the models provide an estimate of the total thermal energy output at wavelengths past 50 μm (0–200 cm^{-1}). This value ranges between 6.76 and 6.80 × 10^{-5} W cm^{-1} ster.$^{-1}$ for the models shown in Fig. 14a. This compares

ORIGINAL PAGE IS
OF POOR QUALITY

closely with a similar estimate by Hanel et al. (1983) of 6.909×10^{-5} W cm^{-2} ster.$^{-1}$, a value which is only some 2% higher on the average. The resonable correspondence of the models to our observations thus provides empirical support for their estimate.

c. Uranus

The temperature structure assumed for the atmosphere of Uranus is shown in Fig. 11 (Tokunaga et al. 1983). The various temperatures near and below the 1-bar pressure level are a direct consequence of various assumptions regarding the mixing ratio of CH_4 in the deep atmosphere (see Appendix E) Among the model spectra shown in Fig. 12, the one with the lowest CH_4 abundance provides the best fit to the observations over the broadest spectral range. The submillimeter data imply a [C]/[H] elemental abundance ratio near or below the Jovian or the solar values. The model provides a satisfactory fit to the 17.8 and 19.6 μm data of Tokunaga et al. (1983). All the models are cooler than the observations of Orton et al. (1983) at 10.3, 11.6 and 12.5 μm, consistent with their interpretation that part of the flux in this spectral region is reflected sunlight. The greatest difficulty associated with the Uranus models is the divergence between the high millimeter brightness temperatures which they predict (for low CH_4 abundances) and the much lower temperature observations in this region (e.g. Ulich, 1981) which would appear to be matched better by the 2% CH_4 model.

The observations form a set which can be used to determine the effective temperature of Uranus. Relying on our data and on models only for the flux at wavelengths smaller than 35 μm, we derive a total flux equivalent to an effective temperature of 58.3 K with an uncertainty of ± 1.5 K from statistical errors and ± 2.0 K from the absolute calibration uncertainty. This value is consistent with previous estimates (Fazio et al 1976; Loewenstein et al. 1977;

ORIGINAL PAGE IS
OF POOR QUALITY

Stier et al. 1978), indicating no measured change in Uranus' effective temperature over this time period.

Lockwood et al. (1983) have derived a Bond albedo of 0.393 $^{+.037}_{-.045}$ for the 1981 epoch and 0.342 $^{+.032}_{-.039}$ for the 1962 epoch. From these estimates, the equilibrium temperatures in 1962 and 1981 are about 57.0 ± 0.8 K and 55.8 ± 1.0 K, respectively. There is sufficient overlap in the uncertainties to support the absence of an internal heat source. Furthermore, recent measurements of the Uranian phase curve by Voyager 1 and 2 camera systems (Wenkert and Danielson, 1982) could be consistent with lower values of the phase curve than previously assumed. The implied drop in the value of the Bond albedo would thus abolish any argument for the existence of an internal heat source.

D. Neptune

The temperature structure assumed for the atmosphere of Neptune is shown in Fig. 13. It corresponds to an optimized fit to our data as a result of perturbing the models of Tokunaga et al. (1983), which is also shown. As for Uranus, various CH_4 mixing ratios in the deep atmosphere result directly in the various temperature structures at and below the 1-bar level shown in Fig. 13. The model spectra, shown in Fig. 14, demonstrate that only the model with the lowest CH_4 abundance comes closest to matching data across the widest spectral range, just as for Uranus. The 17.8 and 19.6-μm observations of Tokunaga et al. (1983) are fit well, although the 10.3 μm observation of Orton et al. (1983) is brighter than the thermal spectra models, supporting the possibility that reflected solar radiation is contributing substantially to the observed flux at that wavelength. Similar to the case for Uranus, only a model with a higher CH_4 mixing ratio value does well in matching the 3.3 mm observation of Ulich (1981). This model is also consistent with the 1 mm observation of

Werner et al. (1978).

Finally, we used the observations to improve the evaluation of the effective temperature of Neptune. The models imply values between 60.1 K and 59.8 K, depending on bulk composition assumptions. Using our data and models only to estimate the total flux at wavelengths short of 35 μm, we derive a total flux equivalent to an effective temperature of 60.3 K with ± 1.5 K uncertainty from statistical errors and ± 2.0 K from the absolute calibration uncertainty. This value is larger than that derived by Loewenstein et al. (1977a), but is extremely close to the value derived by Stier et al. (1978).

Newburn and Gulkis (1972) suggest a Bond albedo for Neptune which is approximately the same as for Uranus, based on the similarity of their spectra, and Murphy and Trafton (1974) suggest a similar value. Values of 0.33 or 0.34 would imply an equilibrium temperature of about 45 K; our estimate of the planetary effective temperature thus implies an internal heat source on the order of 2.56 times the amount of absorbed solar energy. If lower values for the phase integral are adopted, consistent with the Voyager 1 and 2 observations of Neptune's phase curve (Wenkert and Danielson, 1982), then the magnitude of the internal heat could be reduced to a number as low as 1.90 times the amount of absorbed insolation.

VI. SUMMARY

The data for Jupiter and Saturn provide measurements of the far infrared output at wavelengths inaccessible to the Voyager IRIS experiment team (Hanel et al. 1980; 1983). They support the conclusions of these authors that the thermal energy fluxes of Jupiter and Saturn are equal to 1.67 and 1.78 times the solar input, respectively, although their estimates of the Bond albedo are quite independent of this wavelength region. For Jupiter, the value is consistent with an interpretation in which all the flux is supplied by

ORIGINAL PAGE IS
OF POOR QUALITY

GRAVITATIONAL AND INTERNAL ENERGY AS A PART OF THE FINAL COOLING AND CONTRACTION PHASE OF EVOLUTION (GRABOSKE ET AL. 1975; BODENHEIMER ET AL. 1980). HOWEVER, FOR SATURN, ADDITIONAL ENERGY IS REQUIRED WHICH CAN MOST PLAUSIBLY BE PROVIDED BY THE PROCESS OF HELIUM DIFFERENTIATION IN THE INTERIOR (E.G. STEVENSON, 1980). THE DATA DO NOT LEND THEMSELVES TO A PARTICULARLY CLEAR DISTINCTION BETWEEN THE MODELS DISCUSSED ABOVE, BUT THEY SUGGEST THAT HIGHER SPECTRAL RESOLUTION DATA COULD DISCRIMINATE BETWEEN THOSE MODELS SHOWN AND OTHERS WITH ATMOSPHERRIC ABSORBERS WHICH WERE NOT INCLUDED EXPLICITY IN THE CALCULATIONS.

THE URANUS AND NEPTUNE DATA TEND TO CONFIRM PREVIOUS ESTIMATES OF THE TOTAL BOLOMETRIC THERMAL FLUX AND TO IMPROVE THEIR INTERNAL ACCURACY. ULTIMATE IMPROVEMENT OF THE ACCURACY OF THE MEASUREMENTS IN THE ABSOLUTE SENSE MUST AWAIT THE DEVELOPMENT OF A CALIBRATION SYSTEM IN THIS WAVELENGTH REGION WHICH IS MORE ACCURATE THAN THE PLANET MARS WITH ITS SYSTEM OF ACTIVE SURFACE-ATMOSPHERIC PHYSICAL CHEMISTRY AND CIRCULATION. THE MEASUREMENTS PROVIDE SUPPORT FOR THE EXISTENCE OF AN INTERNAL HEAT SOURCE IN NEPTUNE AND THE ABSENCE OF ONE IN URANUS; BOTH, IN FACT, EMIT LESS THAN PREDICTED FROM A HOMOGENEOUS COOLING FROM AN INITIAL HOT STATE (HUBBARD AND MACFARLANE, 1980). THIS IS MOST EASILY EXPLAINED BY THE PRESENCE OF UPWARD REDISTRIBUTION OF HEAVIER MATERIALS SOMETIME DURING THEIR THERMAL HISTORIES, THUS DIMINISHING THEIR AVAILABLE EXCESS LUMINOSITIES.

OUR DATA PROVIDE SUBSTANTIAL CONSTRAINTS ON THE TEMPERATURE STRUCTURES OF BOTH URANUS AND NEPTUNE. THE STRUCTURES ADOPTED BY TOKUNAGA ET AL. (1983), BASED ON APPLEBY (1980), ARE ESSENTIALLY CORRECT FOR URANUS AND ABOUT ONE OR TWO DEGREES TOO WARM FOR NEPTUNE IN THE REGION NEAR 300 TO 500 MBAR TOTAL PRESSURE. FOR THE DEEPER CONVECTIVE REGIONS OF BOTH PLANETS, THE SUBMILLIMETER

DATA SUGGEST A STEEP LAPSE RATE. THIS RATE IS INCONSISTENT WITH METHANE MIXING RATIOS AT THE LEVEL OF 1% OR GREATER BECAUSE OF THE PRONOUNCED EFFECTS OF THE LATENT HEAT OF CONDENSATION ON THE ADIABAT FOR SUCH LARGE ABUNDANCES. FURTHER IMPROVEMENTS IN THE INVESTIGATION OF URANUS AND NEPTUNE WOULD BEST BE PROVIDED BY IMPROVEMENTS IN THE ABSOLUTE CALIBRATION SCALE AND HIGHER SPECTRAL RESOLUTION OBSERVATIONS, JUST AS FOR JUPITER AND SATURN. NEW OBSERVATIONS AT MODERATE SPECTRAL RESOLUTION AT WAVELENGTHS SHORTER THAN 30 MICRONS WOULD PROVIDE FURTHER ELUCIDATION OF THE BULK COMPOSITION (HYDROGEN TO HELIUM RATIO) AND THE TEMPERATURE STRUCTURE IN THE 100 TO 400 MBAR RANGE FOR BOTH PLANETS.

ACKNOWLEDGEMENTS

WE THANK THE STAFFS OF THE IRTF AND KAO FOR THEIR ASSISTANCE DURING THE OBSERVATIONS. THIS WORK WAS SUPPORTED BY NASA GRANTS NSG-2057, NAG-W-4, AND NGR 14-001-227. RHH AND RFL WISH TO THANK J. SIMPSON FOR ADDITIONAL MARS MODELING; I. NOLT, HARVEY MOSELEY FOR ALLOWING US TO USE UNPUBLISHED DATA; AND THE STAFF AND CREW OF THE KAO FOR THEIR USUAL SUPERB HELP

GSO ACKNOWLEDGES SUPPORT FROM THE GALILEO PROJECT AND FROM THE PLANETARY ATMOSPHERES PROGRAM OF THE NASA OFFICE OF SPACE SCIENCES AND APPLICATIONS FOR WORK CARRIED OUT UNDER NASA CONTRACT NAS 7-100 AT THE JET PROPULSION LABORATORY, CALIFORNIA INSTITUTE OF TECHNOLOGY. HE ALSO THANKS THE LOS ANGELES SUPERIOR COURT JURY COMMISSIONER FOR OFFICE SPACE DURING A PORTION OF THIS RESEARCH. WE THANK J. HANSEN, N. HABRA AND D. SOLL AT THE NASA GODDARD INSTITUTE FOR SPACE STUDIES FOR COMPUTING SUPPORT; G. BIRNBAUM AND C. CHAPODOS FOR LABORATORY RESULTS IN ADVANCE OF PUBLICATION; AND J. APPLEBY, K. BAINES, J. BERGSTRALH, S. GULKIS, M. KLEIN AND T. THOMPSON FOR USEFUL ADVICE RELEVANT TO THIS WORK.

ORIGINAL PAGE IS
OF POOR QUALITY

APPENDIX A

Partial Resolution of the Planetary Disk

In some cases, especially the observations of Jupiter, the angular radius of the planet is appreciable in comparison with the beam radius. It is therefore necessary to correct the observed signals for partial resolution of the disk, i.e. for a decrease in detection efficiency with increasing displacement from the optic axis. The normalized scans of Mars give the efficiencies, E( ), as a function of the displacement, ϕ. To good approximation these scans can be fitted by gaussians. For a planet of angular radius Φ in which the brightness is a function $B(\alpha)$ of the emission angle α = arc sin (ϕ/Φ), the disk correction is:

$$D(\Phi) = \int_0^{\Phi} B(\alpha)\pi\phi\, d\phi \Big/ \int_0^{\Phi} E(\phi)B(\alpha)\pi\phi\, d\phi. \qquad (A1).$$

i.e., if S = observed signal, then $D(\Phi)S$ = signal which would be observed for a planet of the same luminosity and the same $B(\alpha)$, but with $\Phi \rightarrow 0$.

We have used the assumption $B(\alpha)$ = constant to obtain the corrections shown in Tables II and VI. As an indication of the sensitivity of $D(\Phi)$ to $B(\alpha)$ we have used the 45 μm (Pioneer 10 and 11) values of $B(\alpha)$ determined for Jupiter by Ingersoll et al (1976). We have made fits of smooth curves to their measured values averaged over five zones of latitude. The difference between the corrections for $B(\alpha)$ = constant and for $B(\alpha)$ based on Ingersol et al (1976) is negligible in comparison with our estimate of the error (10%) in $D(\Phi)-1$ due to uncertainties in $E(\Phi)$.

APPENDIX B - EFFECT OF SATURNS RINGS

Voyager 2 measured the temperatures of the A and C rings of Saturn to be 69 K and 85 K respectively (Hanel et al, 1982). At the encounter, the ring

INCLINATION TO THE SUN WAS 8°. AT THE TIME OF OUR OBSERVATIONS THE RING INCLINATION ANGLE TO THE SUN WAS < ± 1°. WE ASSUME THAT THE RING TEMPERATURE WOULD BE SIGNIFICANTLY LESS THAN THE TEMPERATURES MEASURED BY VOYAGER. IN THIS CASE, THE DOMINANT EFFECT OF THE RINGS WOULD BE TO BLOCK THE EMISSION FROM THE DISK. SINCE THE RING INCLINATION TO EARTH WAS ALWAYS LESS THAN 1 7° DURING OUR OBSERVATIONS, THE GREATEST REDUCTION IN THE EFFECTIVE DISK AREA WOULD BE 1.5%. THE CORRECTION IS MUCH LESS FOR $\lambda \gtrsim 300$ µM.

APPENDIX C - SEQUENCE OF GROUND-BASED MEASUREMENTS

THE INDIVIDUAL OBSERVATIONS USED IN THE IRTF INVESTIGATIONS FOLLOWED A REGULAR PATTERN. CONSIDER, FOR EXAMPLE, A SERIES OF OBSERVATIONS OF MARS, JUPITER AND SATURN USING THE SUBMILLIMETER FILTERS CH2 (BROADBAND), AND CH3, CH4, CH5 (NARROWER BAND). WE USE M2, J3, ETC. TO DENOTE OBSERVATIONS OF MARS WITH FILTER CH2, JUPITER WITH FILTER CH3, ETC. AND S(M2), S(M3) ETC. TO DENOTE THE CORRESPONDING SIGNALS.

A SINGLE SERIES WOULD PROCEED IN THE ORDER M2, M3, M4, M5, M2, J2, J3, J4, J5, J2, S2, S3, S4, S5, S2, AND THE ENTIRE SERIES WOULD BE REPEATED AT LEAST ONCE AND USUALLY TWICE. NOTE THAT FILTER CH2 WAS USED BEFORE AND AFTER THE OTHER FILTERS ON EACH PLANET. IT USUALLY TOOK LESS THAN 10 MINUTES TO COMPLETE THE FIVE SUCCESSIVE COUNTS ON A SINGLE PLANET. THE CORRESPONDING CHANGE IN AIR MASS WAS USUALLY < 0.05. HENCE CORRECTIONS FOR CHANGES IN AIR MASS WITHIN THE SET OF FIVE COUNTS WERE ALMOST NEGLIGIBLE. IN COMPUTING RATIOS OF COUNTS SUCH AS S(M3)/S(M2) FOR ONE SERIES WE SIMPLY INTERPOLATED LINEARLY BY AIR MASS BETWEEN THE S(M2) VALUES AT THE BEGINNING AND THE END OF THE SERIES TO FIND A VALUE FOR THE AIR MASS CORRESPONDING TO M3.

THE TIME BETWEEN THE FIRST AND SECOND SERIES FOR A GIVEN PLANET WAS APPROXIMATELY 45 MINUTES. THE CORRESPONDING CHANGE IN AIR MASS, TYPICALLY

~ 0.15, was usually enough to cause a small but measureable change in a signal ratio such as S(M3)/S(M2). Insofar as possible, the observations were timed to give equal air masses for each of the planets when averaged over all observations for one night.

APPENDIX D - ANALYSIS OF IRTF DATA

(1) Broadband Data

The counts obtained with the broadband filters CH2 and MP2 are insensitive to fine structure in the source spectra, they have high statistical accuracy, and they have been repeated often enough to provide well-sampled signal vs. air mass curves. We use these counts to derive brightness ratios for the various planets, and to provide reference points in deriving the shapes of the individual spectra (Section 2).

The steps in the analysis of the broadband data are as follows:

(i) Plot the signals vs. air mass for each planet for each night.

(ii) To those plots, fit the water vapor curves to estimate the zenith water vapor.

(iii) Adjust all the data for a given night to a common line-of-sight water vapor.

(iv) Combine the adjusted values weighting individual counts according to their noise values, using the nominal errors or the mean error, whichever is larger.

(v) Make a chi-squared test of the N adjusted values and increase the error of the combined result by $(\chi^2/N)^{1/2}$ if the reduced chi squared is >1.

(vi) Calculate the ratios of the averages <S(J2)>/<S(M2)> etc. where the counts in the denominators are for the reference planet (Mars, or,

WHERE NECESSARY, AN INTERMEDIATE STANDARD).

(VII) MULTIPLY THE RATIOS BY THE DISK CORRECTION FACTORS SHOWN IN TABLES II AND IV AND BY THE RATIOS OF PLANETARY SOLID ANGLES TO OBTAIN GLOBAL SURFACE BRIGHTNESS RATIOS B(J2)/B(M2) ETC. FOR THE RANGE OF WATER VAPOR OF THESE MEASUREMENTS, THE BRIGHTNESS RATIOS FOR THESE FILTERS ON DIFFERENT NIGHTS ARE IN SATISFACTORY AGREEMENT AND SHOW NO DEPENDENCE ON ZENITH WATER VAPOR: THE EXPECTED RESULT FOR THE BROADBAND DATA, WHATEVER THE FINE STRUCTURE, IF OVERALL THE PLANETS HAVE ROUGHLY RAYLEIGH-JEANS SPECTRA WITHIN THE PASSBANDS OF THE FILTERS (AS ASSUMED IN PREPARING THE WATER VAPOR CURVES).

(VIII) ASSUME A BRIGHTNESS TEMPERATURE FOR THE REFERENCE PLANET FOR THE DATE OF THE OBSERVATION AND CALCULATE A BRIGHTNESS TEMPERATURE FOR THE "UNKNOWN" PLANET.

(IX) COMBINE THE BRIGHTNESS TEMPERATURES FOR THE VARIOUS NIGHTS WITH WEIGHTING AND CHI-SQUARED TESTS AS IN STEPS (IV) AND (V). WE ASSUME NO CHANGE IN GIANT PLANET TEMPERATURES DURING THE PERIOD OF THE OBSERVATIONS. NO CHANGE IS INDICATED BY THE RESULTS.

(2) NARROWER BAND DATA

IN PRINCIPLE, THE PROCEDURE WE HAVE DESCRIBED FOR THE BROADBAND DATA COULD BE USED ALSO TO FIND THE SIGNAL RATIOS S(J3)/S(M3) ETC. AND HENCE THE BRIGHTNESS TEMPERATURES FOR THE NARROWER BANDS. HOWEVER, THE ERRORS IN DETERMINING THE RELATIVE BRIGHTNESSES IN THE VARIOUS PASSBANDS FOR A SINGLE PLANET ARE REDUCED BY THE FOLLOWING PROCEDURE:

(I) CALCULATE $[S(M3)/S(M2)]_W$, $[S(J4)/S(J2)]_W$, ETC., WHERE W = LINE OF SIGHT WATER VAPOR FOR A PARTICULAR MEASUREMENT OF S(M3), S(J4), ETC. AND $S(M2)_W$, $S(J2)_W$, ETC. ARE THE VALUES

OF THE BROADBAND SIGNALS INTERPOLATED TO THE SAME VALUES OF W. THESE RATIOS ARE NOT INDEPENDENT OF W; E.G. S3/S2 DECREASES AND S5/S2 INCREASES WITH INCREASING W. TYPICALLY, THE CHANGE FROM ONE SERIES TO THE NEXT IS 3-10%.

(II) ADJUST THE RATIOS FOR SUCCESSIVE SERIES TO A COMMON VALUE, W_0, USING EMPIRICALLY DETERMINED CORRECTIONS (LINEAR IN W) BASED ON THE DATA FOR ALL RUNS. THE RATIOS THUS DETERMINED AGREE WITHIN STATISTICS. FOR THE SUBMILLIMETER DATA (FILTERS CH2, CH3, N4, CH4, AND CH5) WE CHOOSE $W_0 = 1$ MM. THE RANGE OF VALUES IS $0.3 \le W \le 1.5$ MM. FOR THE MILLIMETER DATA (FILTERS MP2 AND MP4) WE CHOOSE $W_0 = 5$ MM. THE RANGE OF VALUES IS $3.4 \le W \le 6.4$ MM.

(III) COMBINE THE ADJUSTED VALUES TO OBTAIN $\langle S(M3)/S(M2)\rangle_W$, $\langle S(J4)/S(J2)\rangle_W$ ETC. WITH WEIGHTING AND CHI-SQUARED TESTS AS DISCUSSED IN SECTION 1.

(IV) CALCULATE BRIGHTNESS RATIOS RELATIVE TO THE CALIBRATION OBJECT (MARS) USING THE RELATIONSHIPS

$$B(J3)/B(M3) = [B(J2)/B(M2)]/[\langle S(J3)/S(J2)\rangle_W / \langle S(M3)/S(M2)\rangle_W]$$

ETC. AND USING THE VALUES OF B(J2)/B(M2) ETC. AS DISCUSSED IN SECTION 1. NOTE THAT IF THE SMALL ADJUSTMENTS OF STEP (II) ARE CORRECT, THEN THE VALUE OF W_0 WILL NOT INFLUENCE THE CALCULATED VALUE OF B(J3)/B(M3) ETC. THE EFFECTIVE WAVELENGTH IS SLIGHTLY DEPENDENT ON W_0 BUT THE DEPENDENCE IS MUCH WEAKER THAN FOR THE BROADBAND FILTERS.

(V) CALCULATE BRIGHTNESS TEMPERATURES (SEE SECTION 2).

APPENDIX E

Details of Atmospheric Models

Synthetic spectra of Jupiter and Saturn were computed from physical models with 10 cm^{-1} wide elements centered 10 cm^{-1} wide ("flat") elements centered at 99 through 499 cm^{-1} and 5 cm^{-1} wide elements centered at 34 through 99 cm^{-1} for the airborne observations, and 2.5 cm^{-1} wide elements at 9.0 through 34.0 cm^{-1} for the ground-based observations. This approach allowed absorption features such as the manifolds of NH_3 rotation-inversion lines to be resolved.

The opacity of the Jovian atmosphere is dominated by H_2 and NH_3 in the
35 40 μm - 1 mm region. The H_2 collision-induced dipole absorption was calculated using recent models derived for a variety of colliding species: H_2-CH_4 according to Dore et al. (1983), H_2-He according to Cohen et al. (1983). Absorption by NH_3 was calculated using direct integration of inversion and rotation-inversion lines whose spectroscopic parameters are summarized by Husson et al. (1982), based on Husson et al. (1981). Additional gaseous absorption by PH_3 and CO was modelled using line parameters given by Husson et al. (1982).

The radiative transfer calculations were performed using the matrix operator algorithm of Grant and Hunt (1969) in a multiple-layer approximation which used twenty homogeneous layers per decade of pressure change to simulate the gradual change of atmospheric properties with altitude. Direct integration of line absorption was performed using the method of Scott (1974) as modified by Orton (1981).

The temperature structure of Jupiter used in the calculations was adopted from the neutral atmosphere inversion of the Voyager Radio Subsystem (RSS) occultation experiments (Lindal et al. 1981), assuming respective molar

ORIGINAL PAGE IS
OF POOR QUALITY

fractions of 89% and 11% for H_2 and He (Gautier et al. 1981). Ammonia was assumed to have a molar mixing ratio of 2.2×10^{-4} in the deep atmosphere (Lindal et al. 1981) with depletion of higher levels owing to saturation equilibrium and photochemical destruction as modelled by Orton et al. (1982a). The vertical distribution of PH_3 was represented by a maximum mixing ratio of 6×10^{-7} with a gradual depletion with altitude above the 1 bar level, following the profile derived by Kunde et al. (1982) from Voyager IRIS spectra. A constant CO mixing ratio of 2.5×10^{-9} was assumed, an average of the approximate results of Beer (1975) and Larson et al. (1978). We note that the influence of PH_3 and CO lines on the spectrum in 10.0 cm^{-1} through 2.5 cm^{-1} resolution elements appeared to be small.

The temperature structure of Saturn used in the calculations was derived from the results of the planet-wide averaged temperature structure determined from the Voyager IRIS data given by Hanel et al. (1983), with temperatures deeper than 350 mbars derived from the preliminary neutral atmosphere inversion of the Voyager IRIS occultation experiment (Tyler et al. 1982) after adjustment of the bulk composition to 93% H_2 and 7% He (Gautier et al. 1983). Ammonia was assumed to have a molar mixing ratio of 2×10^{-4} in the deep atmosphere. An alternative value of 5×10^{-4} was tested, following models limits given by Klein et al (1978), and was found to affect our spectra negligibly. Depletion of NH_3 at high levels followed saturation equilibrium. A simple model for the vertical distribution of PH_3 was used: a constant mixing ratio of 1.5×10^{-6}, roughly consistent with the results of Tokunaga et al. (1980) and Courtin et al. (1981), with a cutoff near the base of the stratosphere. We discovered that the presence or absence of stratospheric PH_3 was not significant for our calculations. For consistency with Jupiter, we

ASSUMED A CONSTANT CO MIXING RATIO OF 2.5×10^{-9}, ALTHOUGH ITS INFLUENCE ON OUR CALCULATIONS OF THE SATURNIAN SPECTRUM WAS EXTREMELY SMALL, AS THE CASE FOR JUPITER.

WE ALSO TESTED VARIOUS PHYSICAL MODELS FOR NH_3 ICE CLOUDS IN THE JOVIAN ATMOSPHERE FOLLOWING THE GENERAL SCHEME USED BY ORTON ET AL. (1982B). THE PARTICLES ARE CHARACTERIZED BY A MODE RADIUS WHICH IS LEFT A FREE PARAMETER, A 10% VARIANCE IN THE PARTICLE SIZE DISTRIBUTION, AND A SCATTERING PHASE FUNCTION TAKEN FROM FITTING THE NH_3 PARTICLE PHASE FUNCTION OBSERVED IN THE LABORATORRY WITH VISIBLE LIGHT (HOLMES, 1981; HOLMES ET AL., 1980) USING THE POLLACK AND CUZZI (1980) SEMI-EMPIRICAL ALGORITHM FOR IRREGULARLY-SHAPED PARTICLES. NO CLOUD PARTICLES WERE ASSUMED HIGHER THAN THE 100-MBAR TEMPERATURE MINIMUM OR DEEPER THAN THE 630-MBAR SATURATION LEVEL. THE VERTICAL DISTRIBUTION WAS PARAMETERIZED BY PARTICLE SCALE HEIGHT TO GAS SCALE HEIGHT RATIOS OF 0.50, 0.15 AND 0.05. INDICES OF REFRACTION FOR NH_3 ICE WERE TAKEN FROM MARTONCHIK ET AL. (1983) WHICH ARE BASED PRIMARILY ON THE ABSORPTION MEASUREMENTS OF SILL ET AL. (1980). FOR VERY LOW FREQUENCIES ABSORPTION WAS EXTRAPOLATED EXPONENTIALLY DOWNWARD WITH DECREASING FREQUENCY, CONSISTENT WITH THE LOWEST AVAILABLE FREQUENCY MEASUREMENTS OF SILL ET AL. THIS TREATMENT IGNORES POSSIBLE PHONON ABSORPTIONS, SUCH AS OCCUR IN WATER ICE (E.G. MISHIMA ET AL. (1983), OWING TO THE ABSENCE OF RELEVANT LABORATORY DATA. OTHER RESTRICTIONS ON THE PARTICLE SIZE AND VERTICAL SCALE HEIGHT DETERMINED BY ORTON ET AL. (1982B) WERE ALSO OBSERVED. PHYSICAL MODELS FOR CLOUDS IN THE SATURNIAN ATMOSPHERE SIMILAR TO THOSE FOR JUPITER AND TO THOSE INVOKED FOR SPATICALLY-RESOLVED OBSERVATIONS OF SATURN (ORTON, 1983) WERE NOT INVOKED, AS DISCUSSED IN THE MAIN TEXT.

THE 35-100 μM SPECTRA OF URANUS AND NEPTUNE ARE EXPECTED TO BE DOMINATED BY THE COLLISION-INDUCED ABSORPTION OF H_2, AND THE COMPARISON WITH MODEL

spectra tend to support this view. At this time, there is no evidence to suggest that non-continuous features should be present in the spectrum. For Uranus (and Neptune) the low temperatures eliminate NH_3 at detectable levels, unless present in abundances exceeding saturation equilibrium by many orders of magnitude. Phosphene should also be depleted by saturation equilibrium, although not as much as ammonia. While carbon monoxide may not be depleted by a similar process, its influence on the measurements should be very small if its mixing ratios in Uranus and Neptune are similar to Jupiter. We therefore assumed that the spectrum could be described well by the continuum due to H_2. Thus, direct comparisons between the computed spectrum and the brightness temperatures given in Table II at various wavelengths are physically meaningful.

For the temperature structures for Uranus and Neptune, we followed a procedure adopted by Orton et al. (1983) which examines existing models by Tokunaga et al. (1982). Their temperature structures are partially based on radiative-convective equilibrium models of Appleby (1980) and are constrained to match 17.8 and 19.6 μm observations. The temperature structures characterizing their models were perturbed in a way which optimized the fit to
35 our data between 40 and 100 μm.

As a baseline composition, we assumed a mixing ratio of 90% for H_2, close to those for Jupiter and Saturn. The remainder was assumed to be composed of He and CH_4. CH_4 influences the thermal spectrum in two ways. First, CH_4 collisions with H_2 change the H_2 collision-induced dipole absorption spectrum for that produced by H_2 or He collisions. Second, CH_4 condensation in the upper troposphere lowers the dry adiabatic lapse rate via latent heat (e.g. Eq. 3 of Wallace, 1980). The extent of this wet adiabat is controlled by the

amount of CH_4 in the deep, uncondensed atmosphere. Three values for this mixing ratio were tested: 0.2%, 2% and 4%. The first is close to the Jovian value (Gautier et al. 1982), the second is an arbitrary "intermediate" value, and the last is a value recommended by Baines (1983). Values as high as 10% have been suggested for Uranus (Danielson, 1977), but these were judged by Orton et al. (1983) to be unlikely.

The approximate agreement between the shape of the model spectra of Uranus and Neptune and the data argues that the compositional assumptions implicit in the model are not unreasonable. The data in the 10 - 12 μm regions could be fit better by thermal emission alone if the molar fraction of He were increased substantially (e.g. to 50%), but this is considered unlikely. Increasing the He mixing ratio substantially from the values used in the models tends to supress the H_2 rotational features at 16 and 27 μm, flatten the brightness
35 temperature spectrum between 40 and 100 μm, and increase the rise in the brightness temperature with longer wavelengths. The slow variation of temperature with altitude, combined with the limited data set make it impossible to determine a trustworthy value for the He mixing ratio at this time, as in Gautier et al. (1981) for the Voyager IRIS spectra of Jupiter. On the other hand, it is clear that the immediate effect of replacing a substantial portion of the equilibrium H_2 by normal H_2 in the model is to increase the absorption in the 100 - 200 μm range relative to shorter wavelengths, making it much more difficult to fit both spectral regions simultaneously.

Some caution is warranted at this point. First, we are extending the models for H_2 collision-induced absorption well below the lowest temperature at which measurements have been made (cf. Dore et al. 1983), and the uncertainty involved in such an extrapolation is difficult to estimate on a reliable

QUANTITATIVE BASIS. OTHER CHANGES IN THE SHAPE OF THE GENERAL CONTINUUM WOULD TAKE PLACE UNDER THE INFLUENCE OF CLOUDS IN THE ATMOSPHERE IF THE PARTICLE SIZE WERE SUFFICIENTLY LARGE, AS MAY OCCUR IN THE ATMOSPHERE OF JUPITER WITH NH_3 ICE PARTICLES (ORTON ET AL. 1982). FINALLY, CHANGES IN THE HE MIXING RATIO OR THE ADDITION OF NORMAL-H_2 TO EQUILIBRIUM-H_2 IN THE MODEL WOULD CHANGE THE EFFECTIVE SPECIFIC HEAT OF THE ATMOSPHERE AND INFLUENCE THE TEMPERATURE LAPSE RATE IN THE CONVECTIVE (ADIABATIC) PART OF THE ATMOSPHERE FOR PRESSURES GREATER THAN ABOUT 400 MBAR. SUCH CHANGES WOULD INFLUENCE THE BRIGHTNESS TEMPERATURE INCREASE FOR WAVELENGTHS OF ABOUT 200 μM AND ABOVE AND COMPLICATE THE SIMPLE ASSOCIATION WE HAVE PRESENTED BETWEEN THE BRIGHTNESS TEMPERATURES IN THE SUBMILLIMETER AND THE MIXING RATIO OF CH_4 IN THE DEEP ATMOSPHERE.

REFERENCES

APPLEBY, J. F (1980). UNPUB. PH.D THESIS, S.U.N.Y AT STONY BROOK

DAVIES, M E., ABALAKIN, V. K., CROSS, C. A., DUNCOMBE, R. L., MASURSKY, H., MORANDO, B., OWEN, T. C., SEIDELMANN, P. K., SINCLAIR, A. T., WILKINS, G. A. AND TJUFLIN, Y. C. (1980). REPORT OF THE IAU WORKING GROUP ON CARTOGRAPHIC COORDINATES AND ROTATIONAL ELEMENTS OF THE PLANETS AND SATELLITES. CELESTIAL MECHANICS 22 205.

ELLIOT, J. L. (1979). STELLAR OCCULTATION STUDIES OF THE SOLAR SYSTEM. ANN REV. ASTRON. ASTROPHYS. 17, 445.

ELLIOT, J. L., DUNHAM, E., MINK, D. J. AND CHURMS, J. (1980). THE RADIUS AND ELLIPTICITY OF URANUS FROM ITS OCCULTATION OF SAO 158687. ASTROPHYS. J. 236, 1026.

ELLIOT, J. L., FRENCH, R. G., FROGEL, J. A., ELIAS, J. H., MINK, D. J. AND LILLER, W. (1981). ORBITS OF NINE URANIAN RINGS. ASTRON. J. 86, 444.

HANEL, R., CONRATH, B., FLASER, F. M., KUNDE, V., LOWMAN, ., MAGUIRE, W., PEARL, J. C., PIRAGLIA, J. A., SAMUELSON, R., GAUTIER, D., GIERASCH, P., KUMAR, S., AND PONNAMPERUMA, C. (1979). INFRARED OBSERVATIONS OF THE JOVIAN SYSTEM FROM VOYAGER 1. SCIENCE 204, 972.

HANEL, R., CONRATH, B., FLASER, F. M., KUNDE, V., MAGUIRE, W., PEARL, J., PIRAGLIA, J., SAMUELSON, R., CRUIKSHANK, D., GAUTIER, D., GIERASCH, P., HORN, L., AND PONNAMPERUMA, C. (1982). INFRARED OBSERVATIONS OF THE SATURNIAN SYSTEM FROM VOYAGER 2. SCIENCE 215, 544.

HARPER, D. A. ET AL. (1983).

INGERSOLL, A. P., MUNCH, G., NEUGEBAUER, G. AND ORTON, G. S. (1976). RESULTS OF THE INFRARED RADIOMETER EXPERIMENT ON PIONEERS 10 AND 11. JUPITER ED. GEHRELS, T. (UNIVERSITY OF ARIZONA PRESS) 197.

JAFFE, D. T

KLIORE, A. J., PATEL, I. R., LINDAL, G. F., SWEETNAM, D. N., HOLTZ, H. B., WAITE, J. H. JR., AND MCDONOUGH, T. R. (1980) STRUCTURE OF THE IONOSPHERE AND ATMOSPHERE OF SATURN FROM PIONEER 11 SATURN RADIO OCCULTATION. JOUR. OF GEOPHYSICAL RESEARCH 85, 5857

KUHN, P. M., MAGAZINER, E. AND STEARNS, L. P (1976). AREAL DISTRIBUTION OF WATER VAPOR BURDON ABOVE THE TROPOSPHERE. GEOPHYS. RES. LETT. 3 529.

LINDAL, G. F., WOOD, G. E., LEVY, G. S., ANDERSON, J. D., SWEETNAM, D. N. HOTZ, H. B., BUCKLES, B. J., HOLMES, D. P., DOMS, P. E., ESHLEMAN, V R., TYLER, G. L. AND CROFT, T. A. (1981). THE ATMOSPHERE OF JUPITER: AN ANALYSIS OF THE VOYAGER OCCULTATION MEASUREMENTS. J. GEOPHYS. RES. 86, 8721.

LOEWENSTEIN, R. F., HARPER, D. A., MOSELEY, S. H., TELESCO, C. M., THRONSON, H. A., HILDEBRAND, R. H., WHITCOMB, S. E., WINSTON, R. AND STIENING, R. F (1977A). FAR INFRARED AND SUBMILLIMETER OBSERVATIONS OF THE PLANETS. ICARUS 31 315.

LOEWENSTEIN, R. F., HARPER, D. A. AND MOSELEY, S. H. (1977B). THE EFFECTIVE TEMPERATURE OF NEPTUNE. ASTROPHYSICAL JOURNAL 218, L145

NEUGEBAUER, G., MUNCH, G., KIEFFER, H., CHASE, S. C. JR. AND MINER, E. (1971). MARINER 1961 INFRARED RADIOMETER RESULTS: TEMPERATURE AND THERMAL PROPERTIES OF THE MARTIAN SURFACE. ASTRON. J. 76, 719.

ORTON, G. S (1981)?

SIMPSON, J P., CUZZI, J. N., ERICKSON, E. F., STRECKER, D. W. AND TOKUNAGA, A. T. (1981). MARS: FAR INFRARED SPECTRA AND THERMAL-EMISSION MODELS. ICARUS 48, 230.

SWEETNAM, D. N. (1980). VIKING RADIO OCCULTATION STUDIES OF THE SHAPE OF MARS EOS TRANS. AM. GEOPHYS. UNION 61, #46, P. 1020.

TOKUNAGA, A. T. ET AL. (1982).

TRAUB, W. A. AND STIER, M. T.

TYLER, G. L., ESHLEMAN, V. R., ANDERSON, J. D., LEVY, G. S., LINDAL, G. F., WOOD, G. E., AND CROFT, T. A. (1982). RADIO SCIENCE WITH VOYAGER 2 AT SATURN: ATMOSPHERE AND IONOSPHERE AND THE MASSES OF MIMAS, TETHYS, AND IAPETUS. SCIENCE 215, 553.

WALLACE, L. (1980). THE STRUCTURE OF THE URANUS ATMOSPHERE. ICARUS 43, 231.

WHITCOMB, S. E., HILDEBRAND, R. H. AND KEENE, JOCELYN, STIENING, R. F AND HARPER, D. A. (1979). SUBMILLIMETER BRIGHTNESS TEMPERATURE OF VENUS, JUPITER, URANUS AND NEPTUNE. ICARUS 38, 75.

WHITCOMB, S. E, HILDEBRAND, R. H. AND KEENE, J. (1980). AN F/35 SUBMILLIMETER PHOTOMETER FOR THE NASA INFRARED TELESCOPE FACILITY. P.A.S.P. 92, 863

WRIGHT, E. L. (1976). RECALIBRATION OF THE FAR-INFRARED BRIGHTNESS TEMPERATURES OF THE PLANETS. ASTROPHYS. J. 210, 250.

WRIGHT, E. L. AND ODENWALD, S. (1980). BRIGHTNESS TEMPERATURE OF MARS. BUL. AMER. ASTRON. SOC. 12, 456.

ORIGINAL PAGE IS OF POOR QUALITY

FIGURE CAPTIONS

Figure 1 Transmission curves of the IRTF filters.

Figure 2-5: The brightness temperature results of Table IV (KAO data) and Table V (IRTF data) are plotted for each planet. For a discussion of the errors, see the text. The dashed curve represents an initially assumed spectrum from which the solid curve was derived using these data in an iterative procedure (see text).

Figure 6: The flux results of Table IV are plotted with the final derived curves (solid curves in Figures 2-5). The individual data points are adjusted to a fixed planetary semi-diameter.

ORIGINAL PAGE IS
OF POOR QUALITY

Figure 7 Spectra of Jupiter for models with no NH_3 cloud (upper curve), and for a cloud with Hp/Hg = 0.15 and particle sizes of 30 μm (middle curve) and 100 μm (lower curve). The spectra are computed with resolution element of 10 cm^{-1} through 100 μm (100 cm^{-1}), 5 cm^{-1} between 100 μm and 200 μm (50-100 cm^{-1}) and 2.5 cm^{-1} between 200 m and 1 mm (10-40 cm^{-1}). The spectrum at short wavelengths is taken from whole-disk Voyager IRIS average of Hanel et al. (1981). Tic marks in the upper graph denote the positions of strong lines or manifolds of NH_3 and PH_3.

Figure 8 Spectra of Jupiter for models with Hp/Hg = 0.50 and particle sizes of 10 μm (upper curve) and 100 μm (lower curve). Other symbols are shown as in Fig. 10.

Figure 9 Spectra of Jupiter for models with Hp/Hg = 0.05 and particle sizes of 10 μm (upper curve) and 100 μm (lower curve). Other symbols are shown as in Fig. 10.

Figure 10 Spectra of Saturn for models with various PH_3 mixing ratios. The curves represent spectra of models with the mixing ratio of PH_3 equal to 1.5×10^{-6} (upper curve), 3×10^{-6} (middle curve) and 1×10^{-5} (lower curve). The mixing ratio of NH_3 in the deep atmosphere equals 2×10^{-4}. Spectra are computed with resolution elements as given in Fig. 10. Tic marks in the upper graph have the same meaning as in Fig. 10.

Figure 11 Temperature structures of Uranus used in the models for a 90% mixing ratio of H_2. Each is a perturbation of the profile given by Tokunaga et al. (1982) which is nearly identical to the structures

shown above the adiabatic region. The difference in temperature structures in the troposphere is the result of different wet adiabatic lapse rates associated with a variety of CH_4 mixing ratios in the deep atmosphere as shown.

Figure 12 Spectra of Uranus for 90% H_2 derived from the temperature structures shown in Fig. 15. Only the absorption of the collision-induced dipole of H_2 is considered in the models. Our data are depicted by the filled circles. The 2% and 4% CH_4 spectra are indistinguishable at this scale near 50 µm. From 10.3 to 19.6 µm, the observations of Tokunaga et al. (1983) and Orton et al. (1983) are also shown as open circles.

Figure 13 Temperature structures of Neptune used in the models for a 90% mixing ratio of H_2. Each is a perturbation of the profile given by Tokunaga et al. (1983), shown by the dashed line where different from the rest, optimized to provide a best fit to our data between 40 and 100 µm. The difference in tropospheric temperatures arises for the same reasons as for Uranus (Fig. 14).

Figure 14 Spectra of Neptune for 90% H_2 derived from the temperature structures shown in Fig. 16. Only the absorption of the collision-induced H_2 dipole is considered in the models. Our data are depicted by the filled circles. The 2% and 4% CH_4 spectra are indistinguishable at this scale near 50 µm. From 10.3 to 19.6 µm, the observations of Tokunaga et al. (1983) and Orton et al. (1983) are also shown as open circles.

ORIGINAL PAGE IS
OF POOR QUALITY

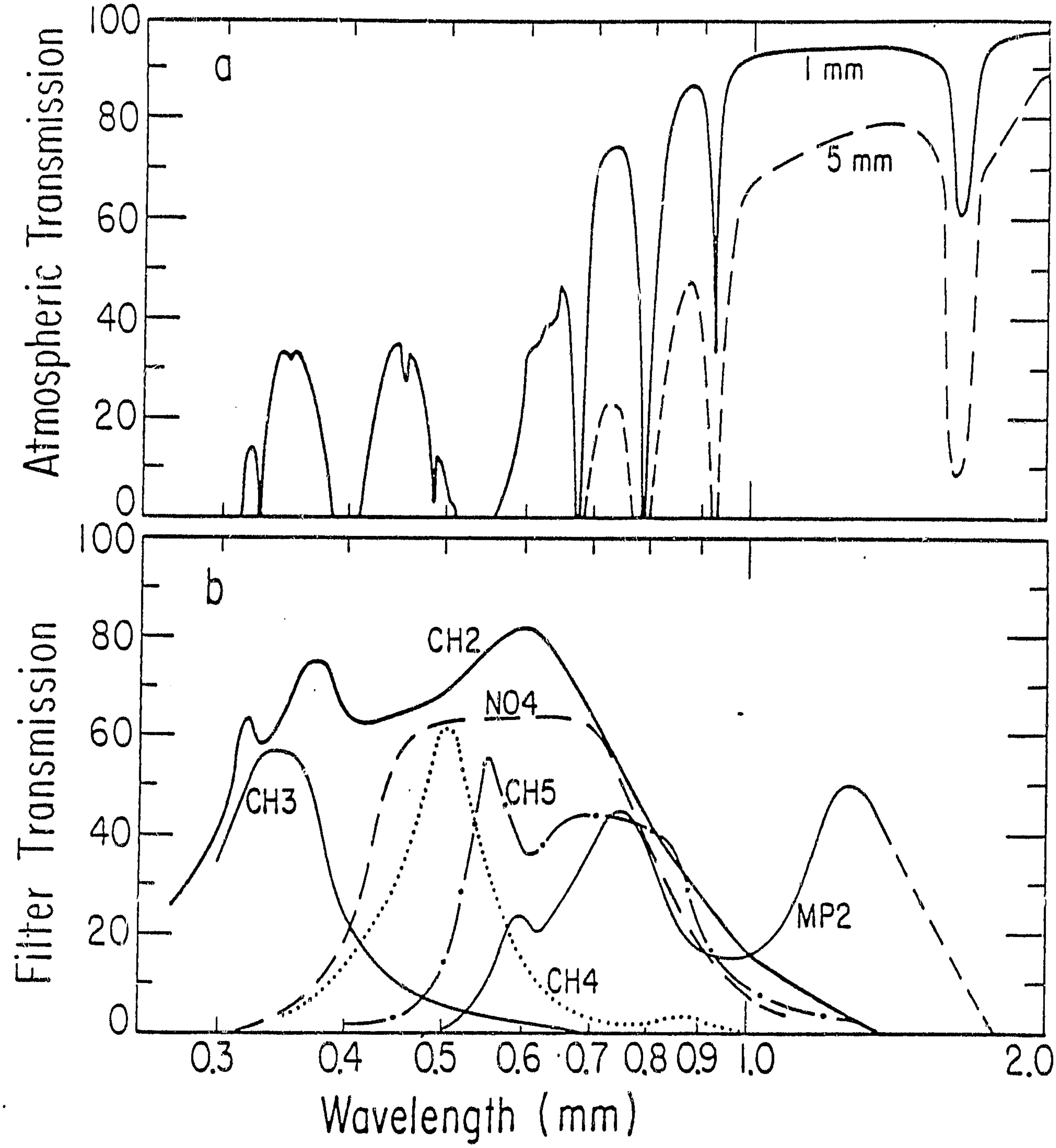

FIG 1

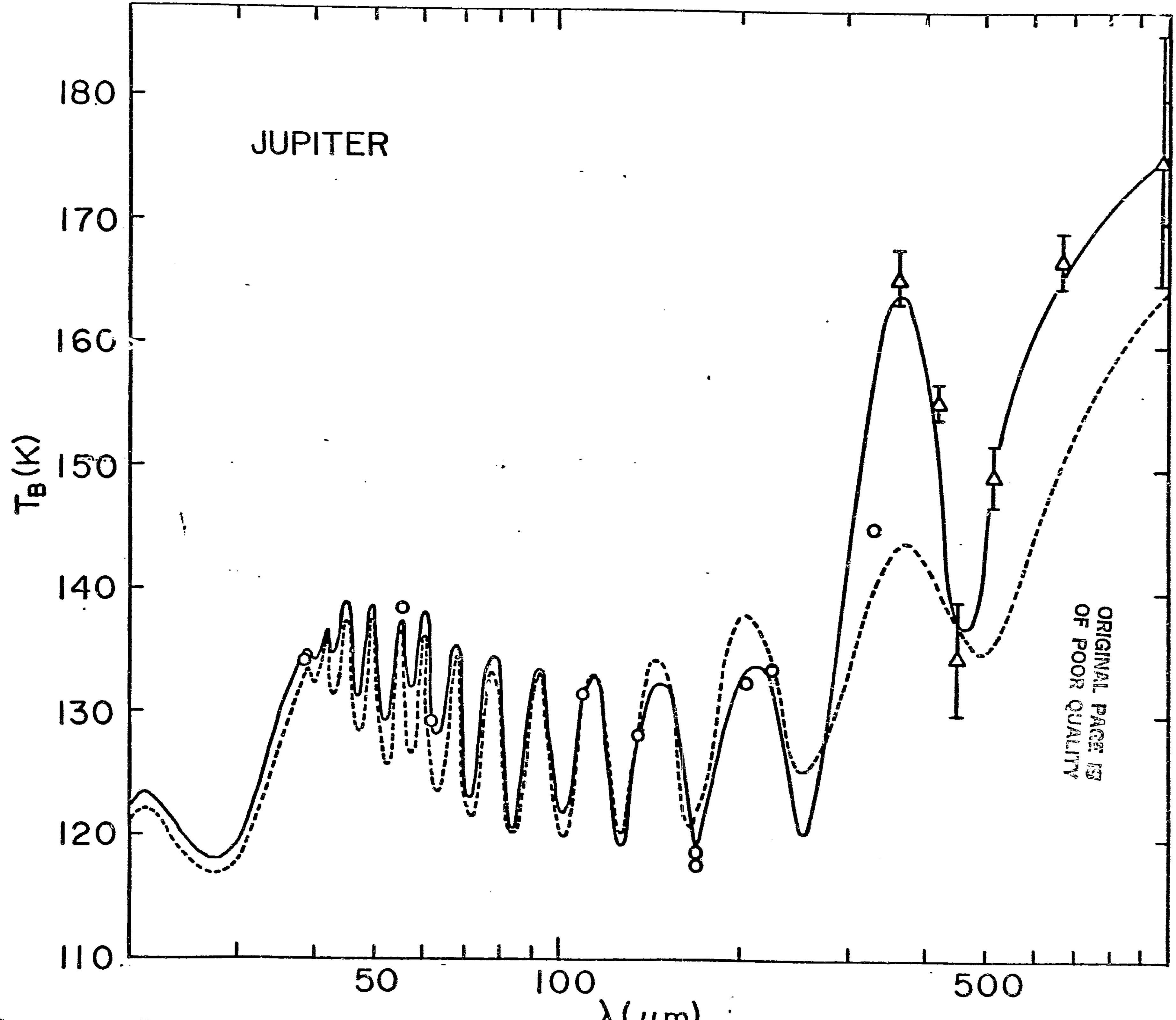
JUPITER
T_B (K)
180
170
160
150
140
130
120
110
50
100
500
λ (μm)
ORIGINAL PAGE IS
OF POOR QUALITY

Fig 2

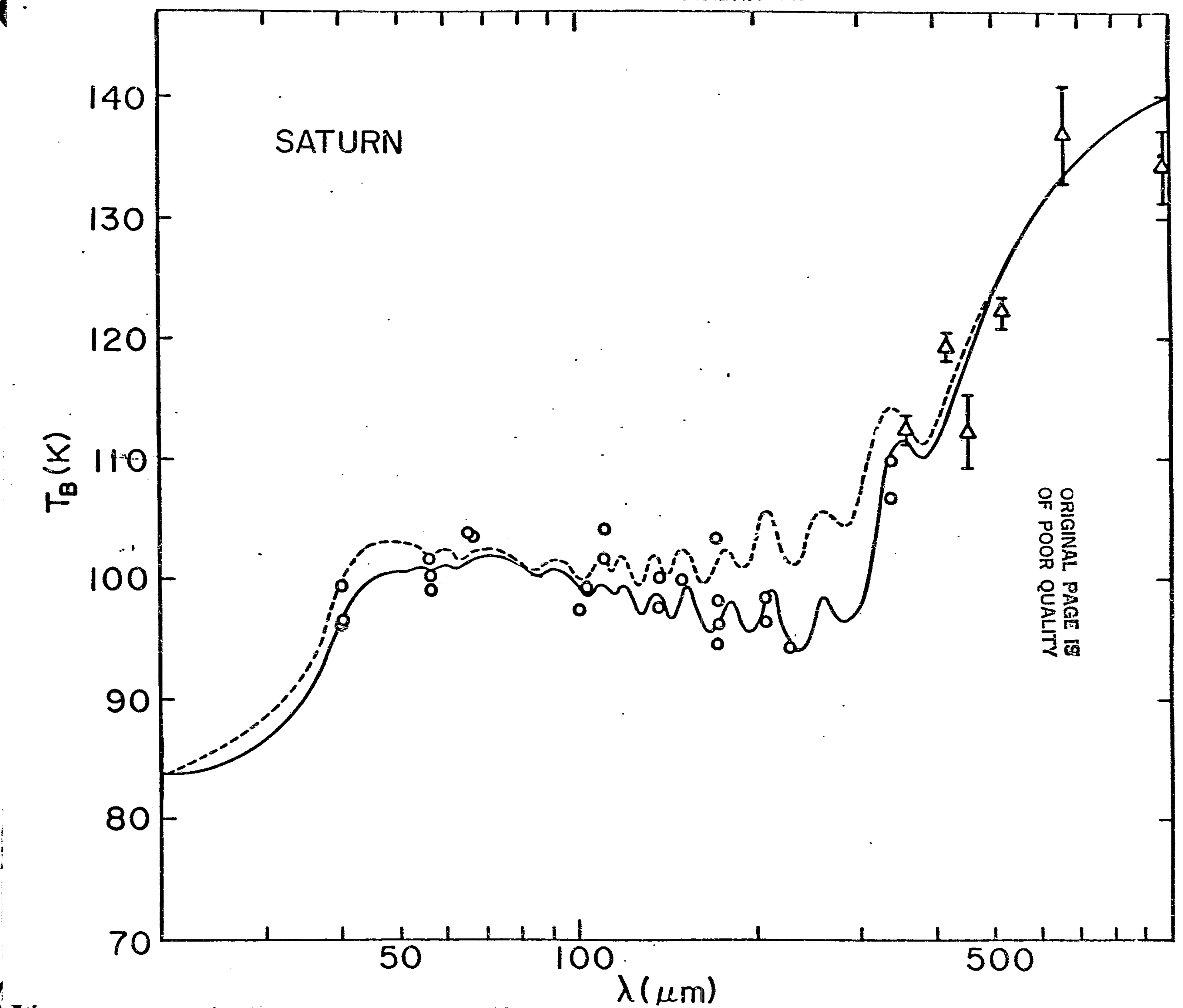
SATURN
ORIGINAL PAGE IS
OF POOR QUALITY
T_B (K)
140
130
120
110
100
90
80
70
50
100
500
λ (μm)

Fig 3.

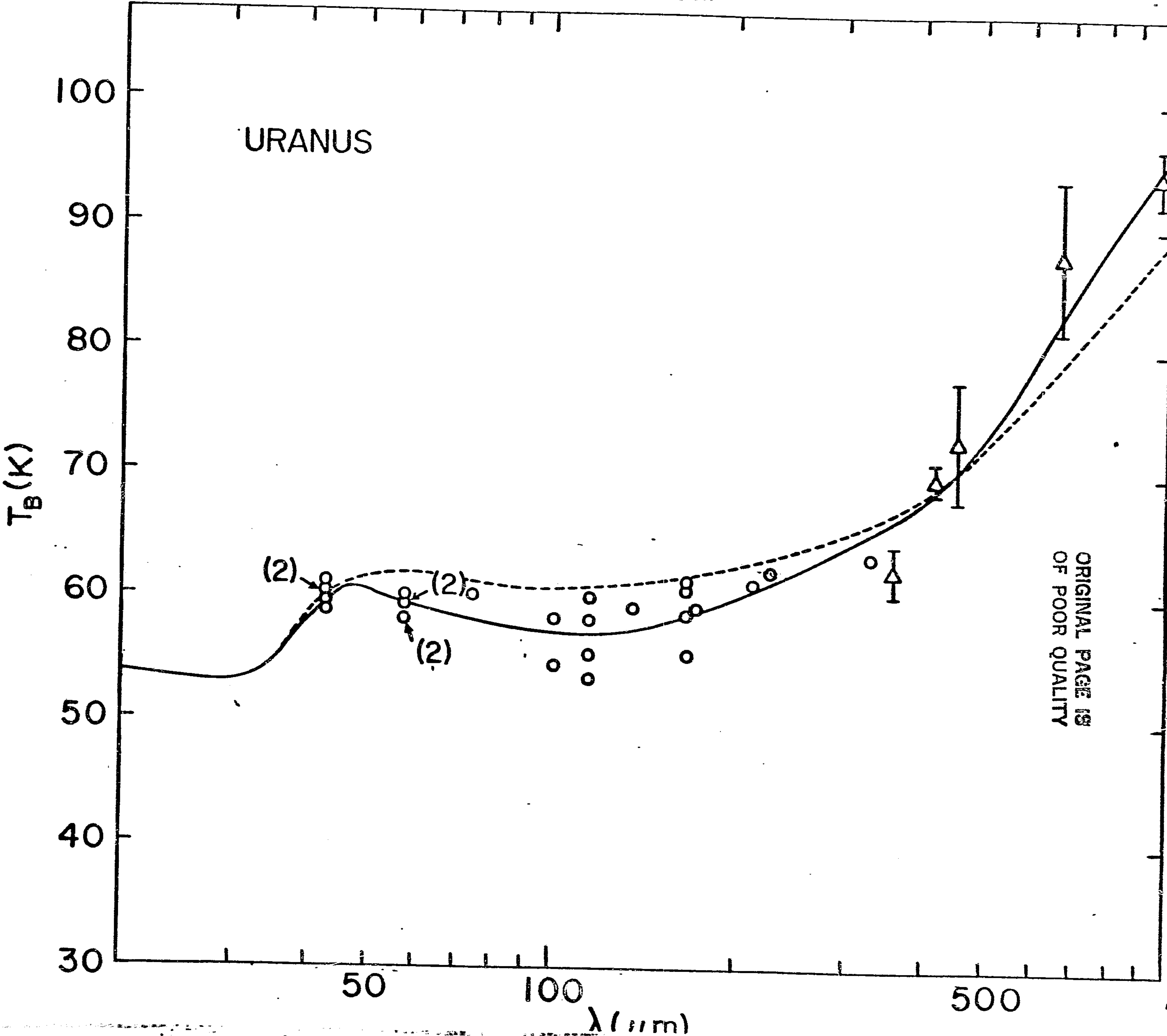

Fig 4

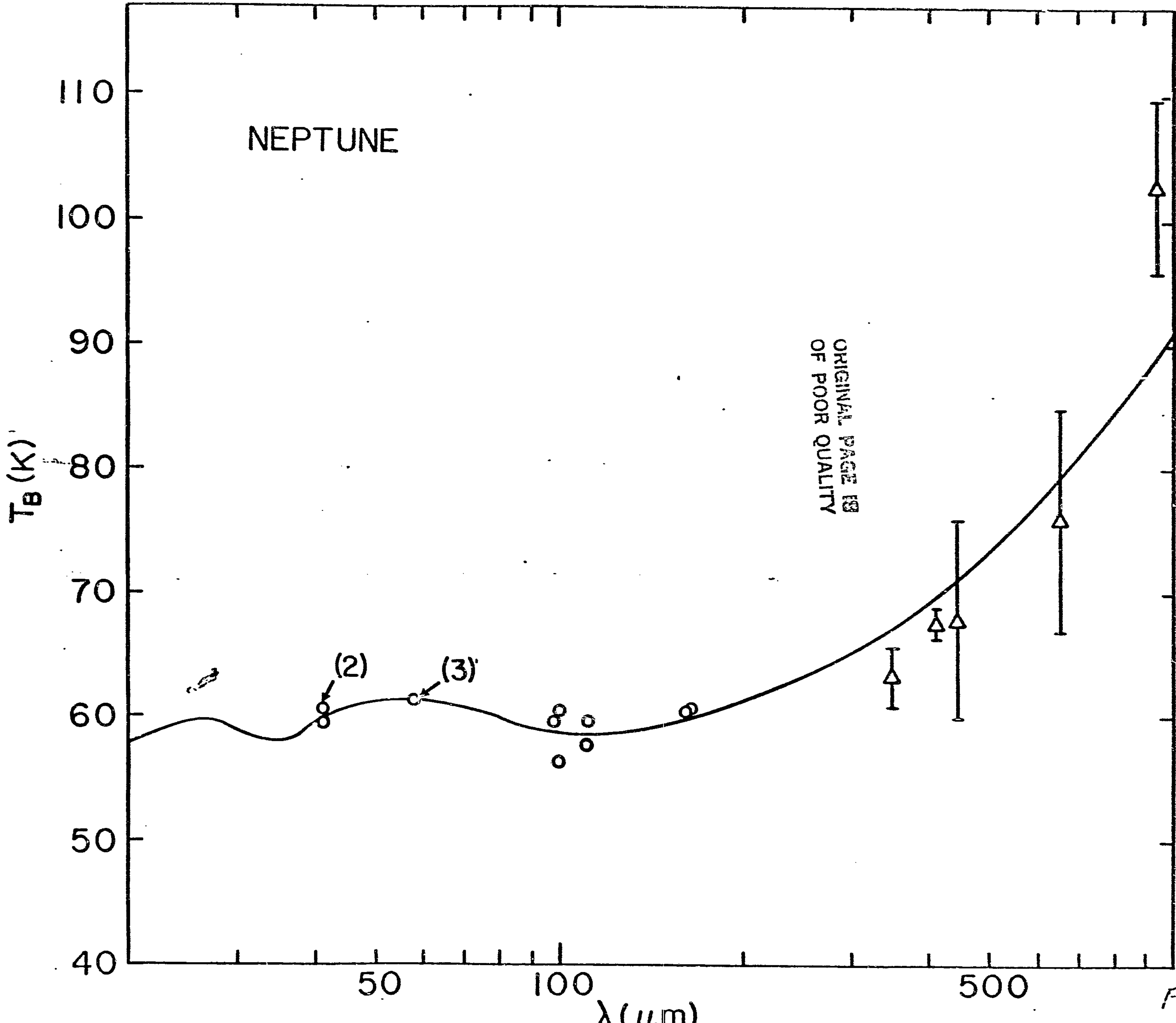

Fig 5

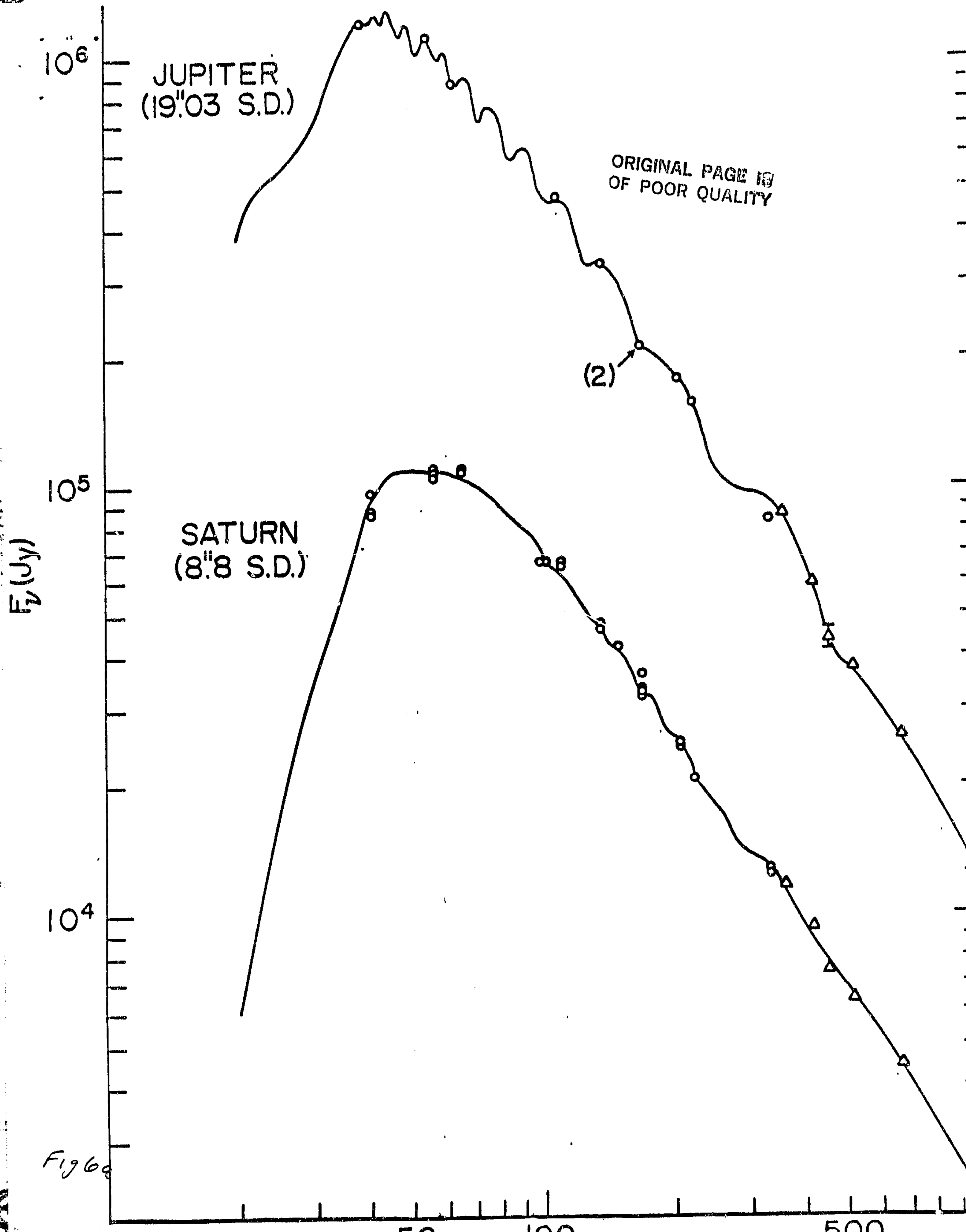

Fig 6a

ORIGINAL PAGE IS
OF POOR QUALITY

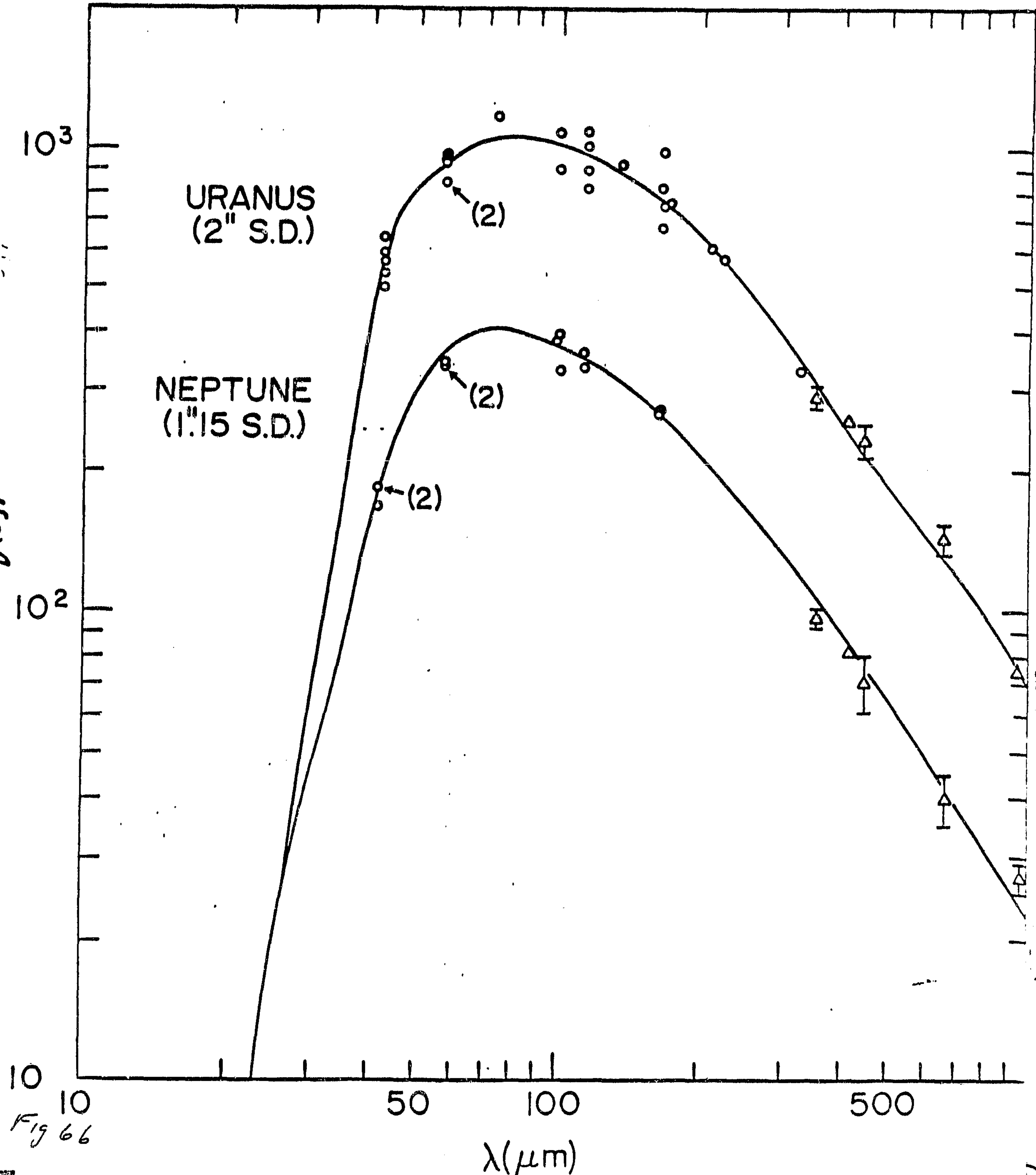

Fig 66

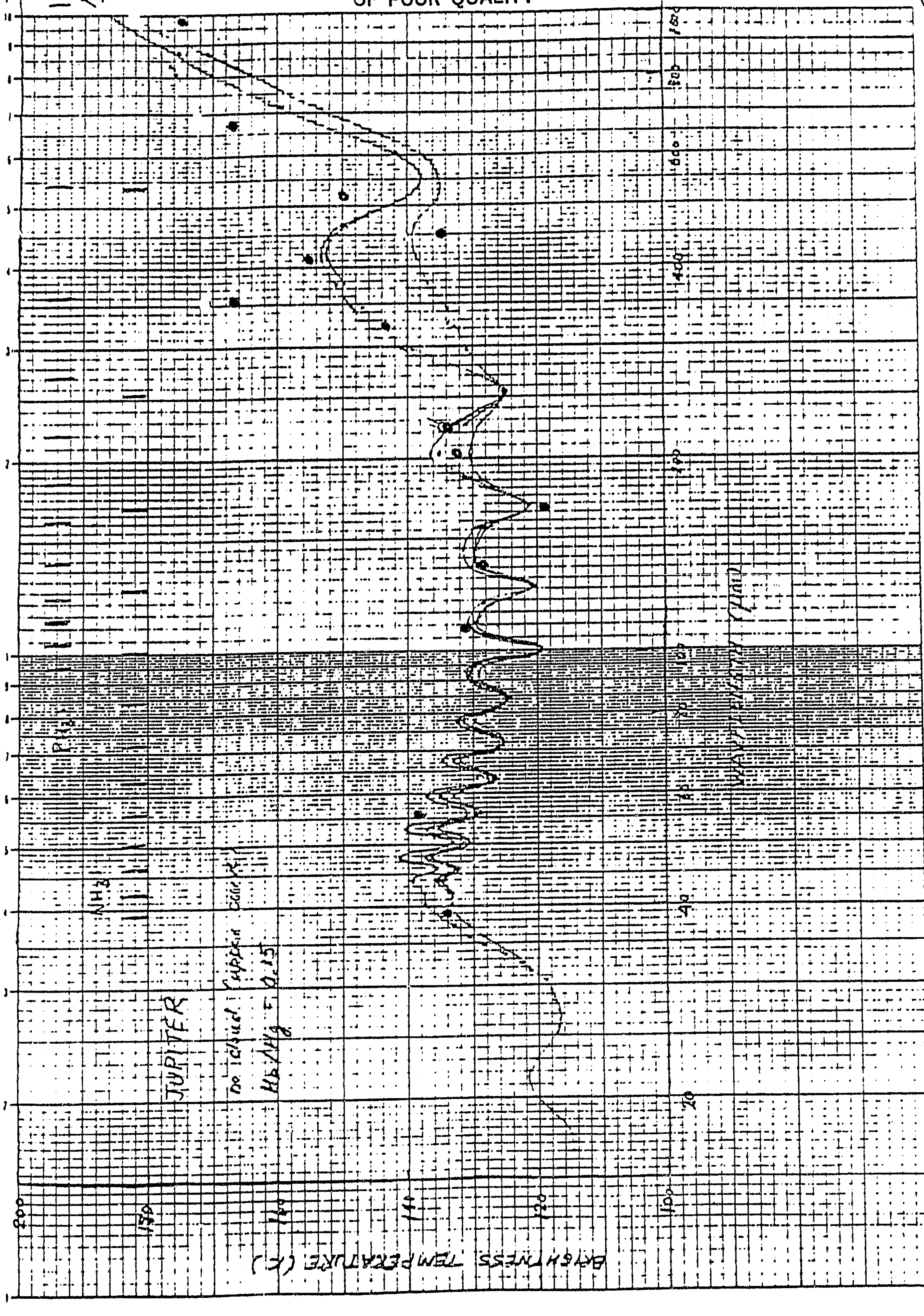
JUPITER
NH3
200
180
160
140
120
100

ORIGINAL PAGE IS
OF POOR QUALITY

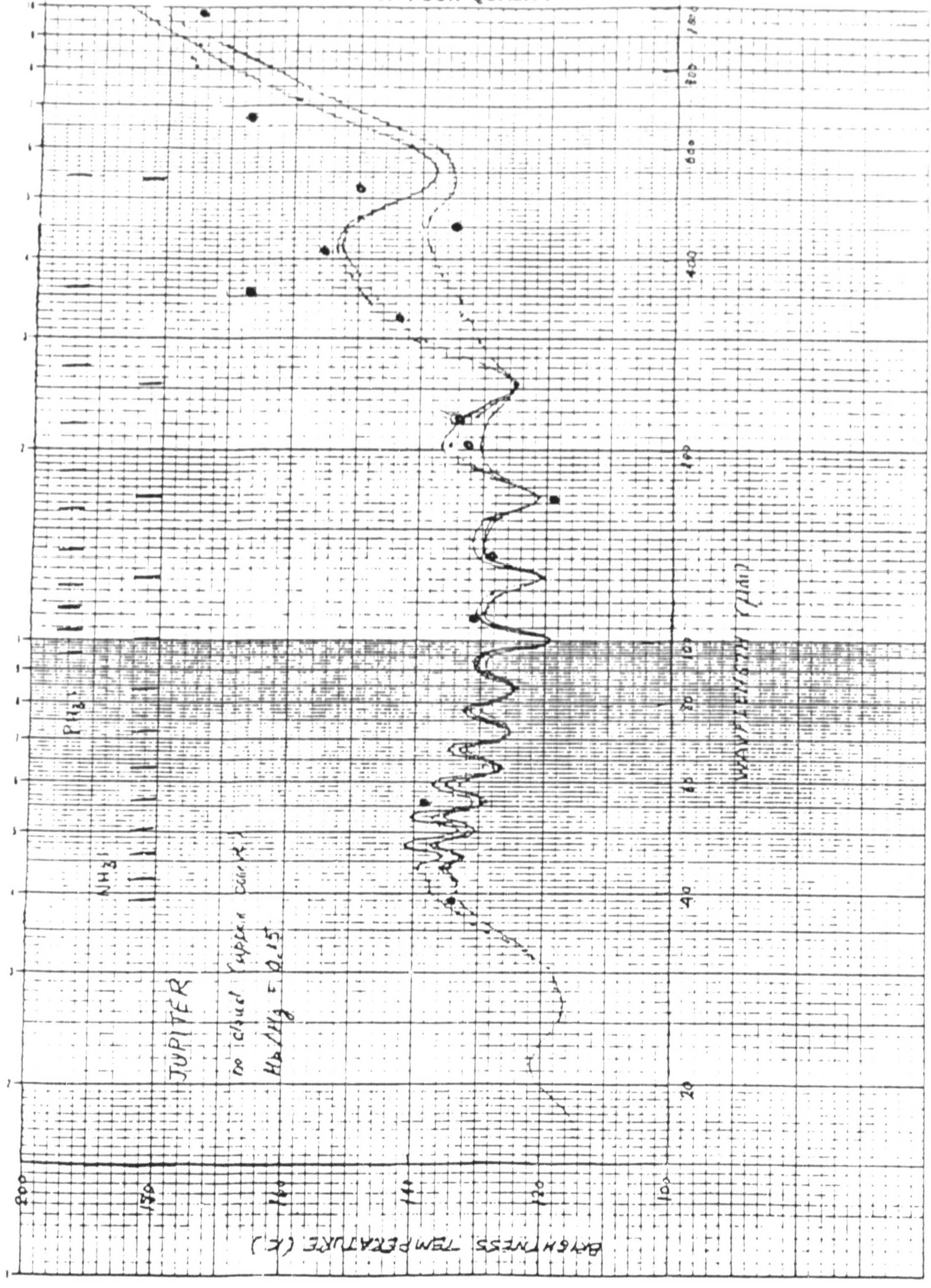

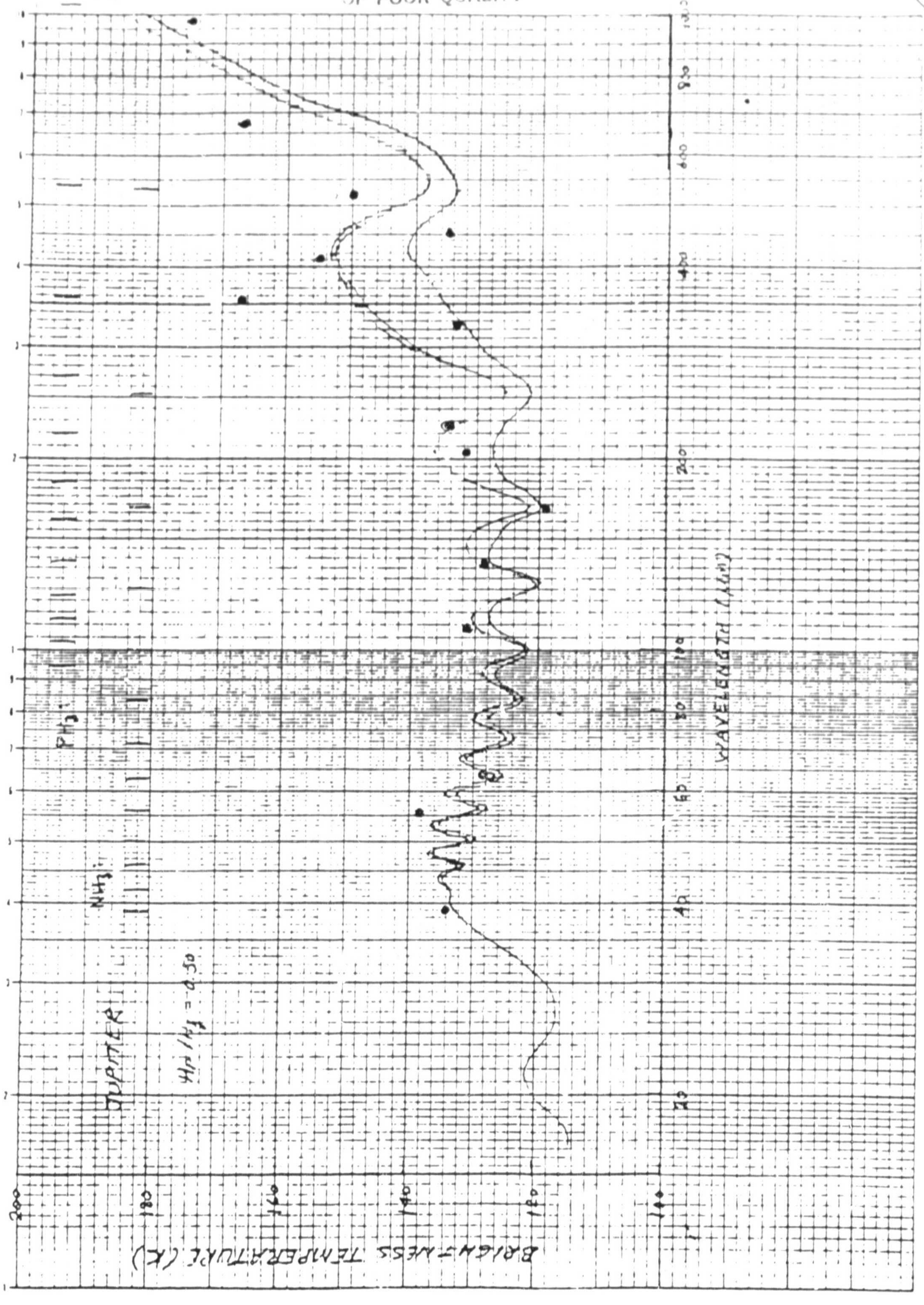
JUPITER
PH_3
NH_3
WAVELENGTH (μm)
BRIGHTNESS TEMPERATURE (K)
200
180
160
140
120
100
20
40
60
80
100
200
400
600
800
1000

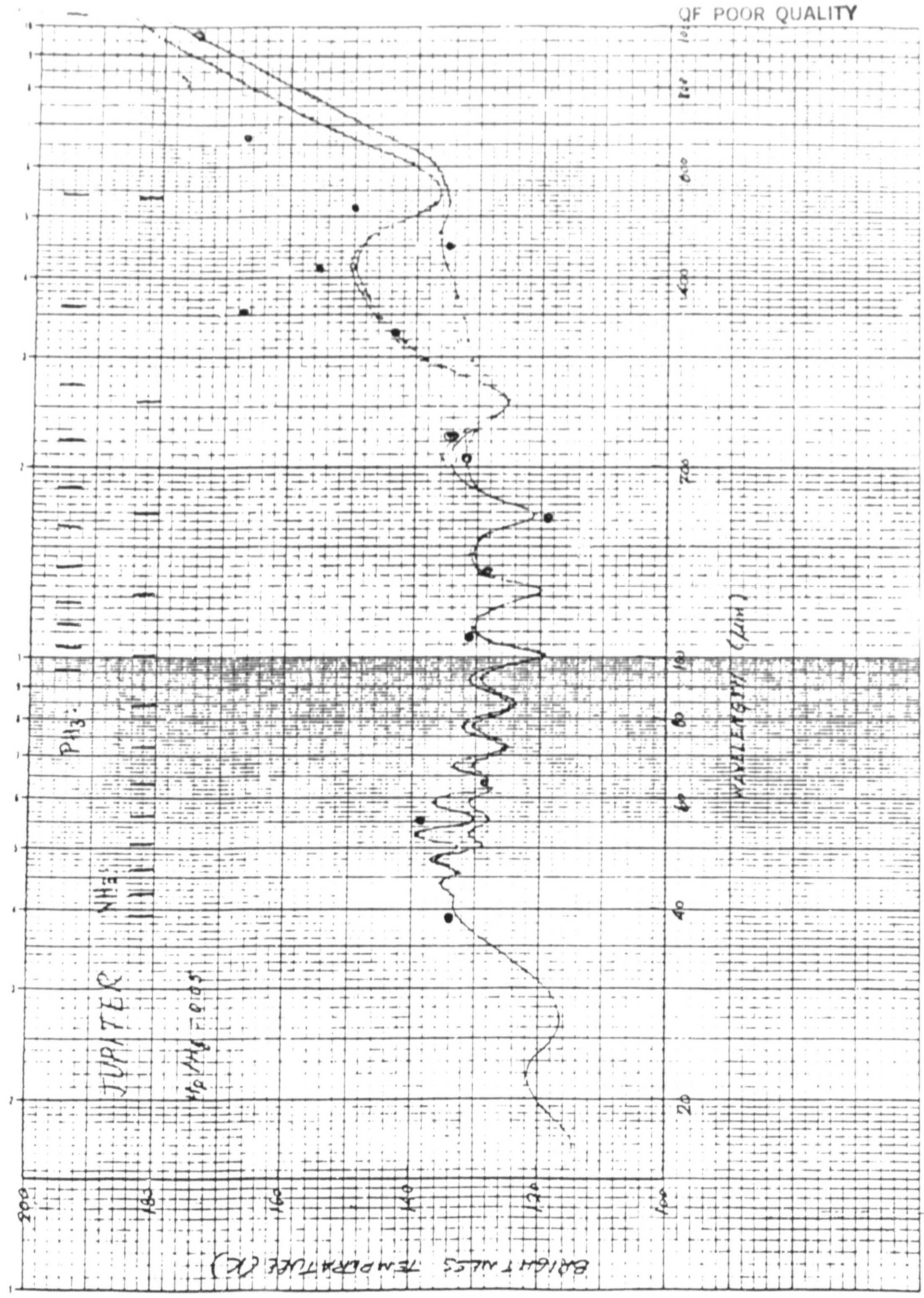
JUPITER
NH_3
P113
WAVELENGTH (μm)
BRIGHTNESS TEMPERATURE (K)
200
180
160
140
120
100
20
40
60
80
100
200
400
600

(10)

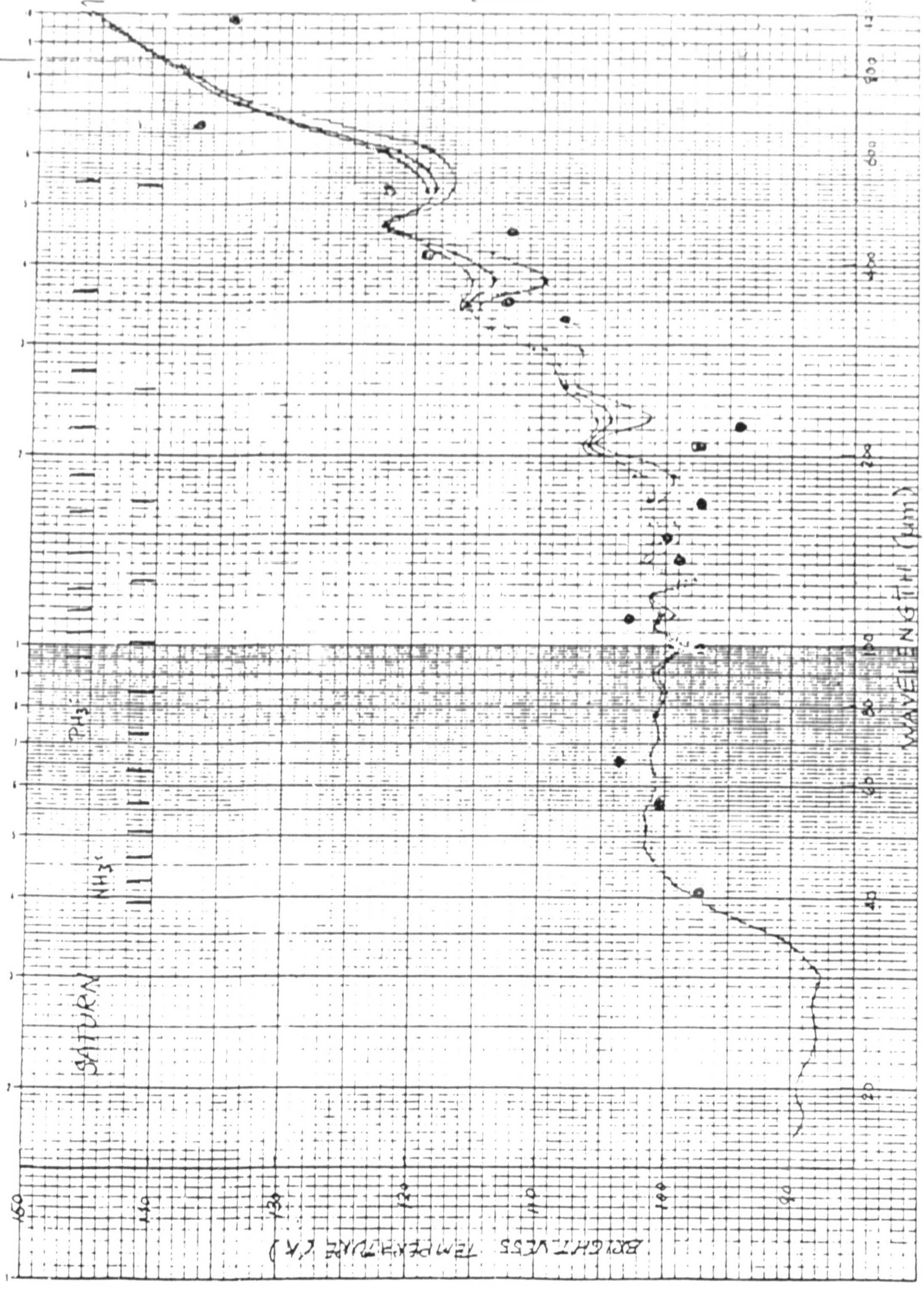
SATURN
NH_3:
PH_3:
WAVELENGTH (μm)
BRIGHTNESS TEMPERATURE (K)
150
140
130
120
110
100
90
20
40
60
80
100
200
400
600
800

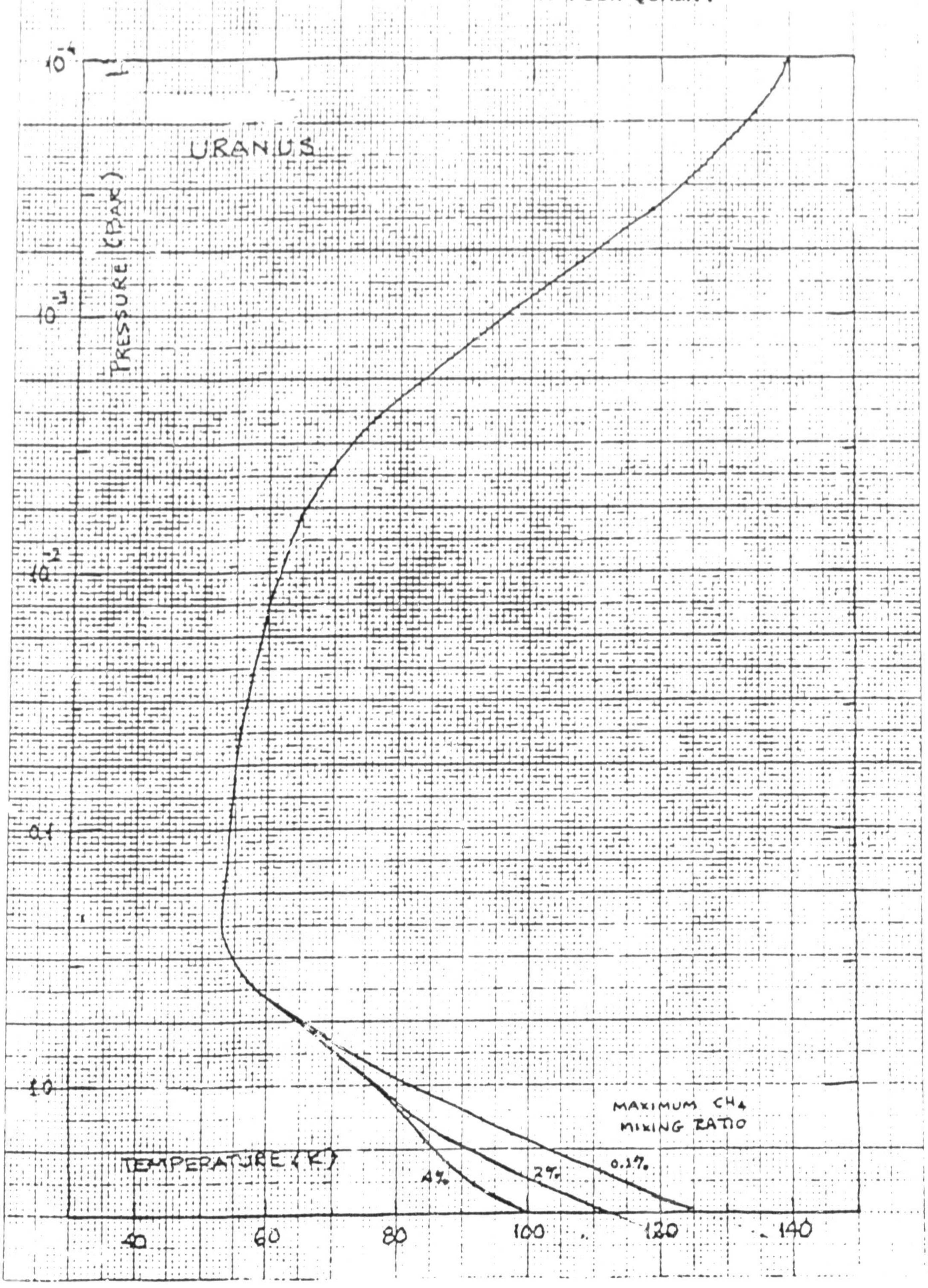
URANUS
PRESSURE (BAR)
10^{-4}
10^{-3}
10^{-2}
0.1
1.0
MAXIMUM CH_4
MIXING RATIO
TEMPERATURE (K)
4%
2%
0.1%
40
60
80
100
120
140

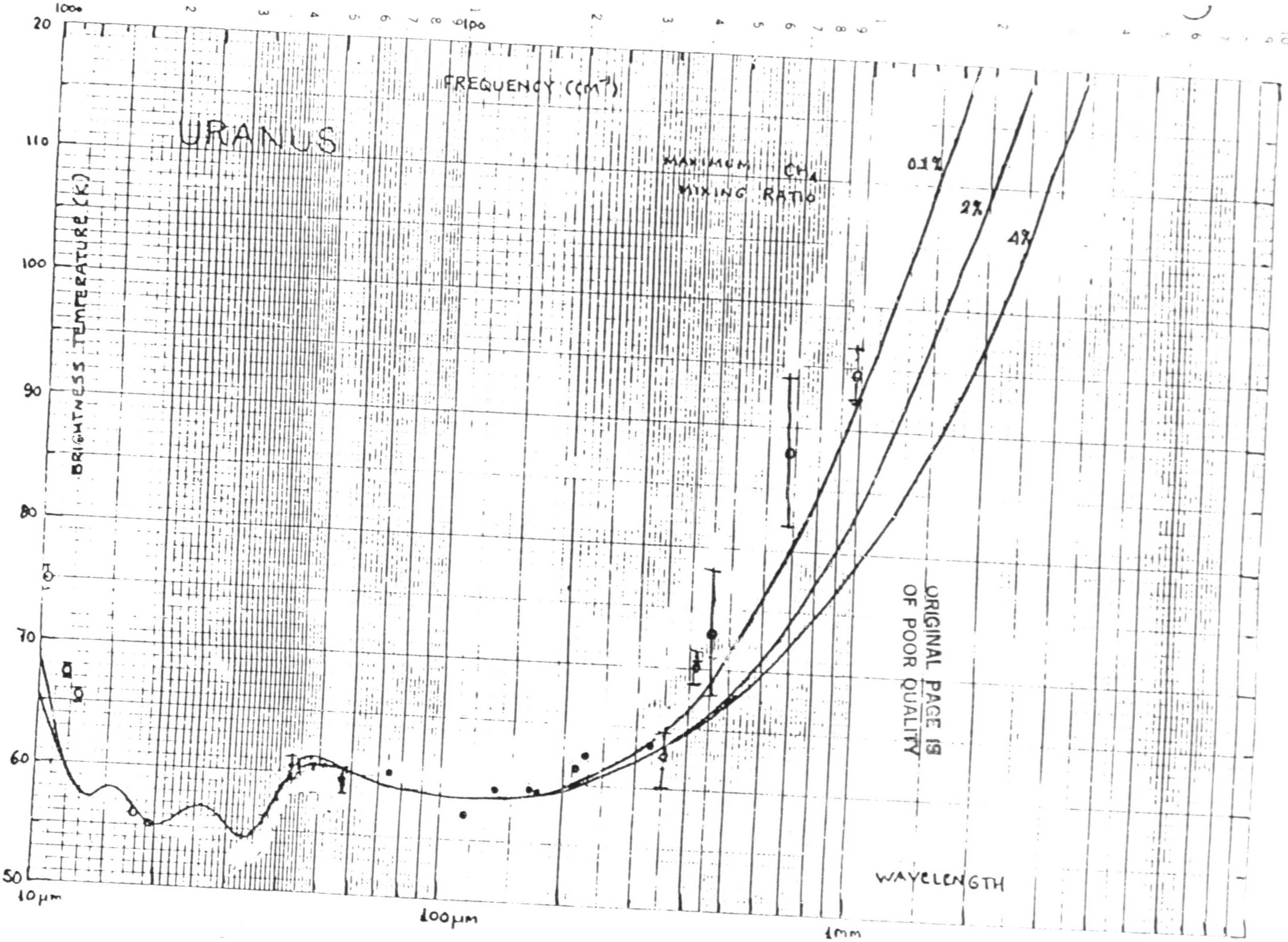

URANUS
FREQUENCY (cm⁻¹)
BRIGHTNESS TEMPERATURE (K)
MAXIMUM CH4 MIXING RATIO
0.1%
2%
4%
WAVELENGTH
10µm
100µm
1mm

(13)

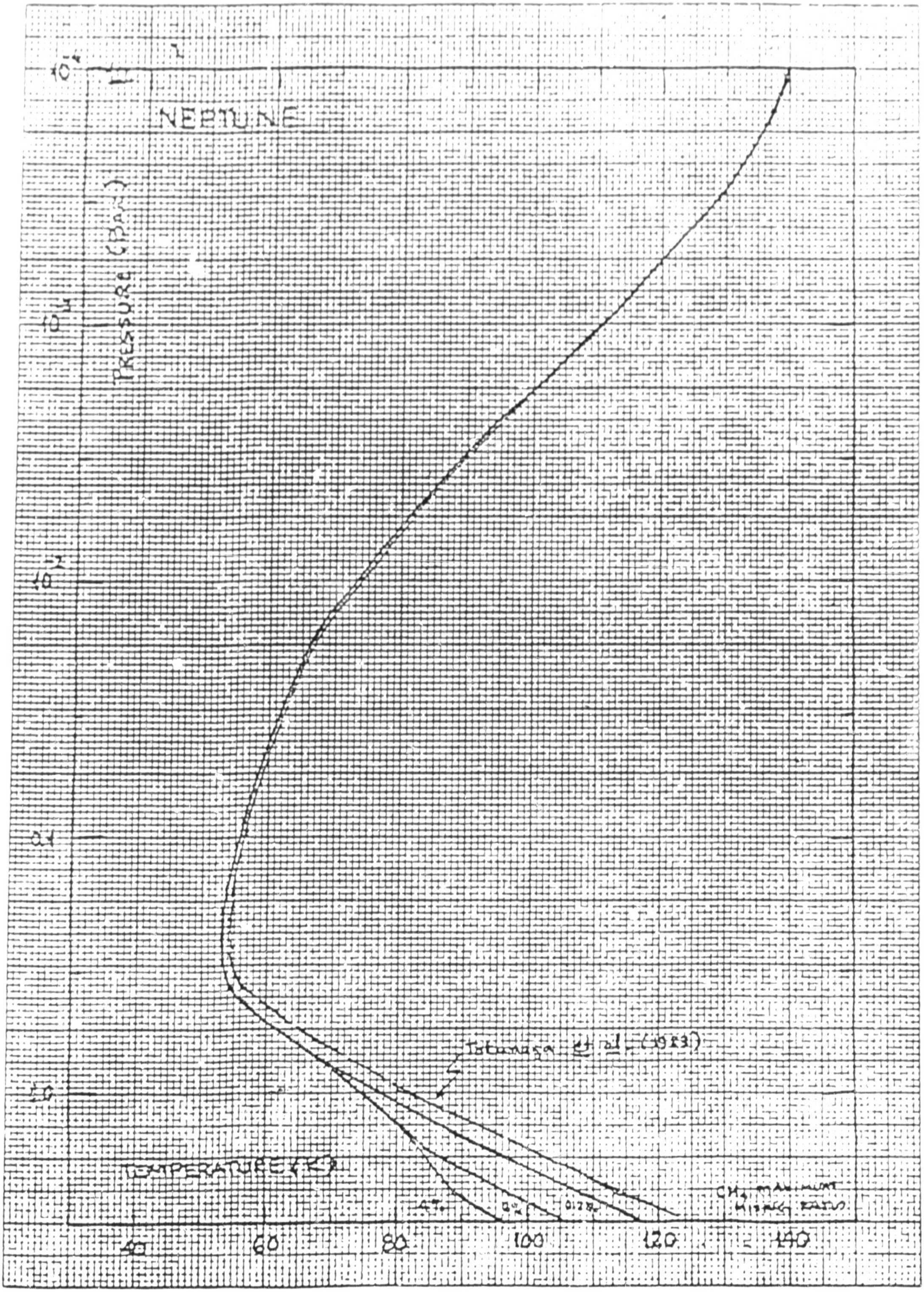
NEPTUNE
PRESSURE (BARS)
TEMPERATURE (K)
Tokunaga et al. (1983)
CH4 MAXIMUM MIXING RATIO
40
60
80
100
120
140

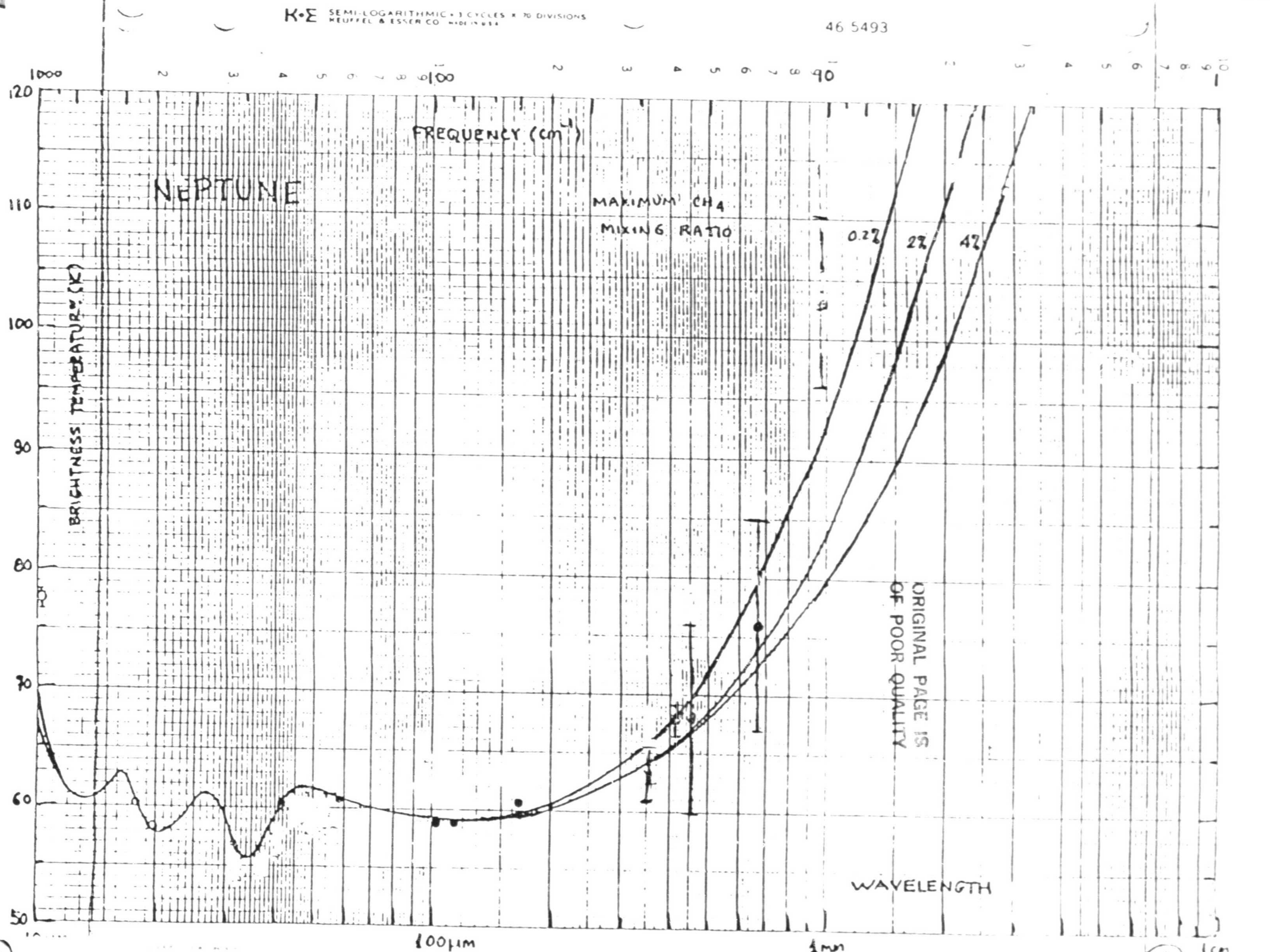

K•E SEMI-LOGARITHMIC • 3 CYCLES X 70 DIVISIONS
KEUFFEL & ESSER CO.
46 5493
FREQUENCY (cm⁻¹)
NEPTUNE
MAXIMUM CH4
MIXING RATIO
0.2%
2%
4%
BRIGHTNESS TEMPERATURE (K)
ORIGINAL PAGE IS
OF POOR QUALITY
WAVELENGTH
100μm
1mm
1cm

(14)